



The Influence of Neural Activity and Neural Cytoarchitecture on Cerebrovascular Arborization: A Computational Model

Bhadra S. Kumar¹, Sarath C. Menon², Sriya R. Gayathri³ and V. Srinivasa Chakravarthy^{1,4*}

¹ Department of Biotechnology, Indian Institute of Technology Madras, Chennai, India, ² Department of Engineering Mathematics, University of Bristol, Bristol, United Kingdom, ³ Indian Institute of Space Science and Technology, Trivandrum, India, ⁴ Center for Complex Systems and Dynamics, Indian Institute of Technology Madras, Chennai, India

OPEN ACCESS

Edited by:

Peter Herman,
Yale University, United States

Reviewed by:

Vassily Tsytarev,
University of Maryland, United States
Sébastien Foulquier,
Maastricht University, Netherlands

*Correspondence:

V. Srinivasa Chakravarthy
schakra@ee.iitm.ac.in

Specialty section:

This article was submitted to
Neuroenergetics, Nutrition and Brain
Health,
a section of the journal
Frontiers in Neuroscience

Received: 10 April 2022

Accepted: 30 May 2022

Published: 04 July 2022

Citation:

Kumar BS, Menon SC,
Gayathri SR and Chakravarthy VS
(2022) The Influence of Neural Activity
and Neural Cytoarchitecture on
Cerebrovascular Arborization:
A Computational Model.
Front. Neurosci. 16:917196.
doi: 10.3389/fnins.2022.917196

Normal functioning of the brain relies on a continual and efficient delivery of energy by a vast network of cerebral blood vessels. The bidirectional coupling between neurons and blood vessels consists of vasodilatory energy demand signals from neurons to blood vessels, and the retrograde flow of energy substrates from the vessels to neurons, which fuel neural firing, growth and other housekeeping activities in the neurons. Recent works indicate that, in addition to the functional coupling observed in the adult brain, the interdependence between the neural and vascular networks begins at the embryonic stage, and continues into subsequent developmental stages. The proposed Vascular Arborization Model (VAM) captures the effect of neural cytoarchitecture and neural activity on vascular arborization. The VAM describes three important stages of vascular tree growth: (i) The prenatal growth phase, where the vascular arborization depends on the cytoarchitecture of neurons and non-neural cells, (ii) the post-natal growth phase during which the further arborization of the vasculature depends on neural activity in addition to neural cytoarchitecture, and (iii) the settling phase, where the fully grown vascular tree repositions its vascular branch points or nodes to ensure minimum path length and wire length. The vasculature growth depicted by VAM captures structural characteristics like vascular volume density, radii, mean distance to proximal neurons in the cortex. VAM-grown vasculature agrees with the experimental observation that the neural densities do not covary with the vascular density along the depth of the cortex but predicts a high correlation between neural areal density and microvascular density when compared over a global scale (across animals and regions). To explore the influence of neural activity on vascular arborization, the VAM was used to grow the vasculature in neonatal rat whisker barrel cortex under two conditions: (i) Control, where the whiskers were intact and (ii) Lesioned, where one row of whiskers was cauterized. The model captures a significant reduction in vascular branch density in lesioned animals compared to control animals, concurring with experimental observation.

Keywords: vascular growth and remodeling, neurovascular development, neurovascular coupling (NVC), whisker barrel cortex, computational model

INTRODUCTION

The neurons in the brain and the cerebrovascular network form a functionally integrated network (Iadecola, 2004). Though the branching and patterning of neural and vascular arbors begin in the fetal stage itself (Carmeliet and Tessier-Lavigne, 2005), the two networks are capable of further growth, remodeling and plasticity postnatally also (Argandoña and Lafuente, 1996, 2000). Electrical activity of the neurons in the brain is highly dependent upon timely and adequate blood supply from the cerebral vascular network; the cerebral blood flow, in turn, is dependent on the vasodilatory signals arising from the neural activity. Therefore, it is understood that there is a bidirectional functional connectivity between the neural and the cerebrovascular system. Hence, there is an anticipation, supported by experimental evidence (Bautch and James, 2009; Lacoste et al., 2014; Lacoste and Gu, 2015), that even the development of both neural and cerebrovascular systems should be interdependent (Andreone et al., 2015; Paredes et al., 2018; Peguera et al., 2021).

Development of the cerebrovascular network is driven by two processes, namely, vasculogenesis and angiogenesis (Coelho-Santos and Shih, 2020). Vasculogenesis is the formation of new vessels from the vascular precursor cells. In contrast, angiogenesis is the formation of new vessels from the existing vessels by a process of branching and arborization, which forms an intricate vascular network. In the embryonic stage, shortly after the closure of the neural tube, between the embryonic day 8.5 (E8.5) and E10, a primitive vascular network is formed around the neural tube. This primitive network of vessels, called the perineural vascular plexus (PNVP), develops in response to the vascular endothelial growth factor A (VEGF-A) released by the neural tube (Hogan et al., 2004; Bautch and James, 2009; James et al., 2009). The proangiogenic nature of VEGF-A activates the vasculogenesis of the neural tube. A variety of cellular and molecular pathways are involved in neurally guided cerebral angiogenesis (Bautch and James, 2009; Paredes et al., 2018; Peguera et al., 2021). In the post-natal stage too, angiogenesis continues to take place and is known to be influenced by the VEGF of neuronal origin (Ogunshola et al., 2000). In addition to angiogenesis of neuronal origin, the angiogenic factors derived from glial cells also influence the vascularization of the central nervous system (Lattera et al., 1990; Lattera and Goldstein, 1991). The glial cells are key players involved in the upregulation and release of VEGF especially during hypoxic conditions (Shweiki et al., 1992; Plate et al., 1994; Wizigmann-Voos et al., 1995; Behzadian et al., 1998). Thus, it can be stated with reasonable confidence that the vascular arborization depends on the neural and glial cytoarchitecture and the preliminary arborization of vessels can be modeled simply using the neural and glial cytoarchitecture data.

The neural architecture and organization in many brain areas indicate the tendency of minimizing wiring costs in the development of neural circuitry (Klyachko and Stevens, 2003; Chklovskii and Koulakov, 2004; Wen and Chklovskii, 2008; Wen et al., 2009). Cuntz et al. (2010) have shown that a variety of dendritic arborization topologies can be accounted

for by the minimum wiring cost principle, a principle that is implemented in the form of a simulation system known as the TREES toolbox (Cuntz et al., 2010). The work of Cuntz et al. (2010) presents a simple algorithm which, by optimizing path length and wirelength, can generate structures strikingly similar to a variety of biologically observed neurons. We propose that the vascular arborization also might be aiming for optimally spanning the tissue volume while ensuring minimal path length and wire length. Given the neural distribution and the vascular growth principle, we show how we can simulate the tree growth architecture that closely matches the experimentally observed vascular arborization characteristics.

Several computational approaches were proposed to model vasculature (Karch et al., 1999; Peyrounette et al., 2018; Li et al., 2020; Shipley et al., 2020; Shabudin et al., 2021). But to the best of our knowledge, there are no computational models that describe the growth and spanning of cerebro-vasculature based on the neural distribution and neural activity. In response to this lacuna, we propose a computational model known as the Vascular Arborization Model (VAM) to understand the effect of activity and density distribution of the neurons on the development of the vascular arborization.

In the first half of the work, we simulate the vascular tree growth in a small volume ($0.1 \text{ mm} \times 0.1 \text{ mm} \times 0.8 \text{ mm}$) of the cortex. The vascular network originates from a parent root node and grows to span the tissue volume based on the cytoarchitecture of the neural and non-neural cells of the cortex. There are two stages of vascular arborization: (i) Growth phase and (ii) Settling phase. In the growth phase, each terminal vessel grows closer to the neurons in its domain such that the mean squared distance between the vascular terminal node and the neurons in its perfusion domain is minimized. When the mean squared distance reaches a minimum, the terminal vessel splits into two smaller vessels. The former perfusion domain is also split into two sub-domains, while the two child terminal vessels now proceed to perfuse the two newly formed subdomains. This process occurring iteratively results in vascular arborization. During the settling phase, the fully grown vascular network is rearranged such that the vascular tree ensures optimal path length and wire length.

In recent studies, it was observed that in addition to the location of neural structures, the neural activity also could influence the vascular patterning (Lacoste et al., 2014; Whiteus et al., 2014; Lacoste and Gu, 2015). Taking this into consideration, in the second half of the work, we modified the VAM model to allow the arborization of vessels depend on neural activity as well. We used a Self-Organizing Map (SOM) model (Kohonen, 1990) to simulate the neural map responses and use it to map the whisker inputs. This neural response was used as the activity in layer 4 (L4) of the whisker barrel cortex. The growth phase was made dependent on neural activity also such that the vessels would not sprout until a minimum neural activity is present in its perfusion domain. The settling phase also was made to depend on the neural activity. We observed the branch point density and vascular volume density in a control model and a lesioned model. The model simulations were close to the experimental observations (Lacoste et al., 2014).

METHODS

The VAM was implemented for a small 3D volume of the somatosensory cortex of the murine brain. The neuronal density distribution of the murine cortex observed experimentally (Tsai et al., 2009) was used to distribute the neurons along the depth of the cortex in the VAM model. The vasculature was initialized as a set of randomly distributed root nodes at the surface of the cortex within the considered volume.

In the phase 1 of the simulation study, we simulate the vascular arborization based on cytoarchitecture of neurons and non-neuron cells, and verified the results obtained using the vascular volume density observed experimentally. Here we considered a smaller section of the somatosensory cortex of dimension $100 \mu\text{m} \times 100 \mu\text{m} \times 800 \mu\text{m}$ which has one single root node.

In the second part of the model, we considered a larger area of the somatosensory cortex $600 \mu\text{m} \times 600 \mu\text{m} \times 700 \mu\text{m}$ with 44 root nodes, and incorporated the neural activity in L4 to make the arborization depend on the activity in addition to cytoarchitecture.

Simulation of Neural Distribution

The neural cell number density along the depth of the cortex was obtained from the Figures 10a–d of Tsai et al. (2009). In phase 1, a volume of dimension $100 \mu\text{m} \times 100 \mu\text{m} \times 800 \mu\text{m}$ was considered, whereas in phase 2, a volume of dimension $600 \mu\text{m} \times 600 \mu\text{m} \times 700 \mu\text{m}$ was considered. The volume was segmented into smaller layers, each of thickness $50 \mu\text{m}$ (dimensions of individual layer in phase 1 are $100 \mu\text{m} \times 100 \mu\text{m} \times 50 \mu\text{m}$, and in phase 2 it is $600 \mu\text{m} \times 600 \mu\text{m} \times 50 \mu\text{m}$) stacked one on top of another along the radial direction of the cortex. The number of neurons in each layer was estimated based on the experimental values of cell number density of neurons at each $50 \mu\text{m}$ depth. Once the number of neurons in each layer was estimated, they were distributed randomly in the layer.

The Vascular Tree Arborization Algorithm Based on Cytoarchitecture

The proposed the vascular tree arborization algorithm consists of two phases:

Phase I: Growth phase,

Phase II: Settling phase.

In Phase I, the tree growth is based on the cytoarchitecture of the neural and non-neural cells (hereafter called “cortical cells”) of the cortex. The vascular tree starts as a single child node starting from a root node. During the growth phase, a single vascular node, emerging from the root node, grows incrementally and splits into branches at appropriate locations ensuring minimum distance between the terminal vessels and the tissues to be perfused. During the settling phase, all the vascular nodes are repositioned such that the tree has an optimal path length and wire length. By pathlength, we define the total distance along the path traced from a leaf node to the root node (in **Figure 1A**, the blue arrows from leaf node to root node trace one path). The wirelength simply denotes the total length of all the

vascular segments in the vascular tree (in **Figure 1A**, each green arrow represents a wire).

Phase I: The Growth Phase

The growth phase describes the process where the rudimentary vascular tree, consisting of a single vascular node, originating from the root node at the cortical surface, grows out, branches and perfuses the tissue volume. The tree which starts its growth from the root node (**Figure 2A**), incrementally grows and spans the space of the tissues such that the average distance between the energy demanding cells (neurons and non-neural cells) and the vascular leaf nodes is minimum.

The total number of cortical cells (neurons and non-neurons), calculated from the cell number density information of the specific region (see Figures 10a–d of Tsai et al., 2009) is represented by N_T . In the smaller volume, $100 \mu\text{m} \times 100 \mu\text{m} \times 800 \mu\text{m}$, estimated N_T ranges between 2000 and 2500 cells and in the larger volume, $600 \mu\text{m} \times 600 \mu\text{m} \times 700 \mu\text{m}$ N_T ranges between 45000 and 50,000 cells based on the region of cortical tissue considered. The total number of nodes in the vascular tree are M_T ($N_T > M_T$). At any given instant during the tree growth, let the set of leaf nodes (terminal vascular nodes) be denoted by LN. Each cortical cell is assigned to the closest node (minimum Euclidean distance) among the m leaf nodes. Given that the coordinate of the j th leaf node is given by Q_j and the coordinate of the i th cortical cell is given by P_i , the sum of squared distance between the i th cortical cell and j th leaf node which is the leaf node closest to the i th cortical cell, denoted by $j(i)$, at any instant is given by,

$$D_j = \frac{1}{2} \sum_{i \in C_j} \|P_i - Q_j\|^2 \quad (1)$$

where C_j is the set of cortical cells assigned to the j th leaf node.

The total distance between the vascular leaf nodes and the cortical cells is given by,

$$D = \sum_{j \in LN} D_j \quad (2)$$

The j th leaf node is moved closer to the cortical cells such that D is minimized

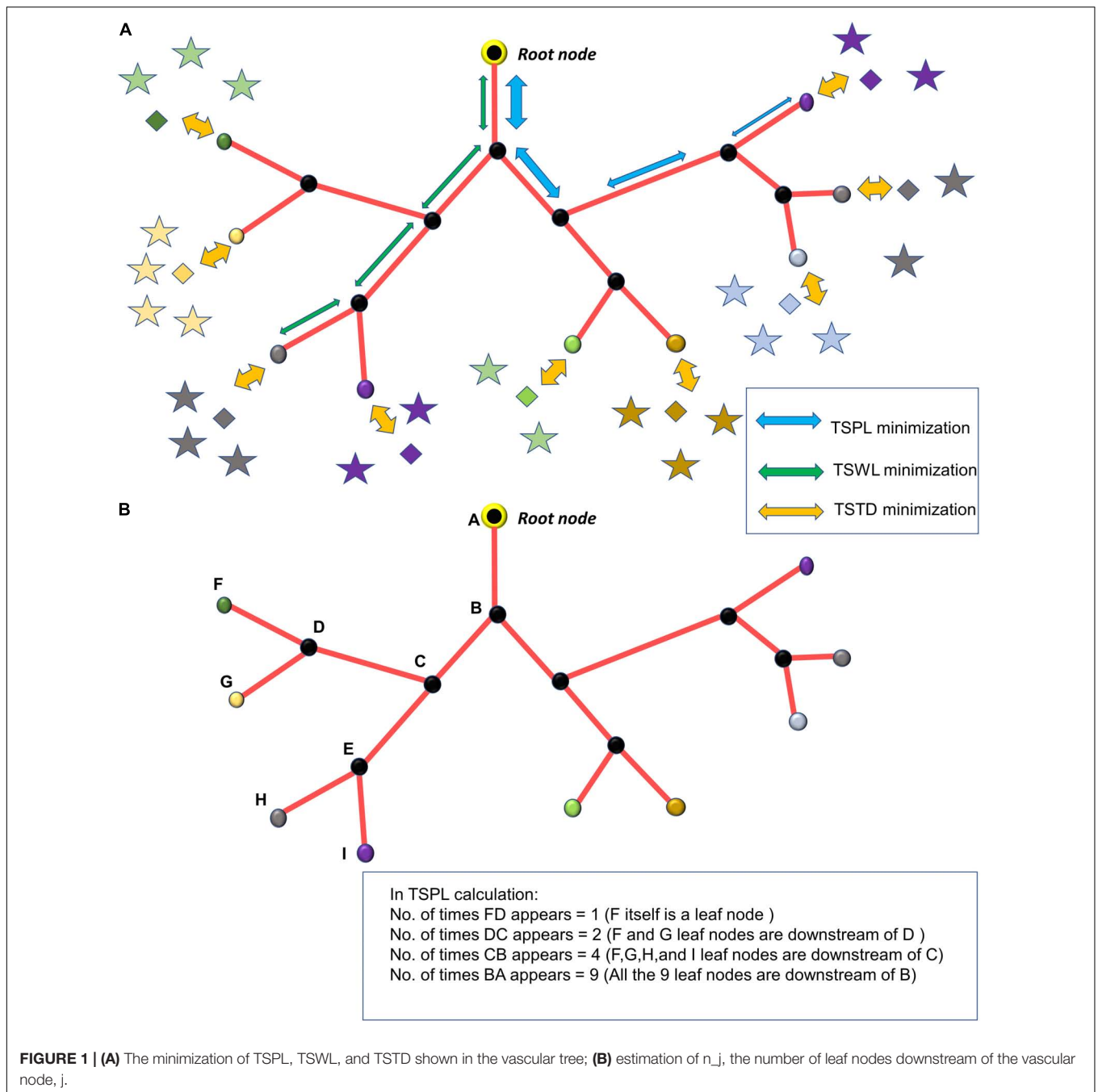
$$\Delta Q_j = -\eta_g \nabla_{Q_j}(D) \quad (3)$$

where η_g is the learning rate.

Given that Q_j is represented by a 3-dimensional vector (x_j^q, y_j^q, z_j^q)

$$\Delta Q_j = -\eta_g \left(\frac{\partial D_j}{\partial x_j^q} + \frac{\partial D_j}{\partial y_j^q} + \frac{\partial D_j}{\partial z_j^q} \right) \quad (4)$$

This gradient is calculated for every $j = 1 : m$. The j th leaf node once reaches a point such that $\Delta Q_j \approx 0$, then the j th node splits giving rise to k child nodes which would be the new leaf nodes. Now the cortical cells are reassigned to the newly formed leaf nodes (**Figures 2B,D**) based on the nearest distance criterion. The new leaf nodes continue to grow like before (**Figure 2C**). The



tree growth terminates when the number of vascular terminal leaf nodes count up to a predefined fraction of the total neurons. That is, the branching stops when $m = n * \alpha$, where $\alpha \leq 1$. The level (l) of a vessel is identified by the number of branchings that occurred from the root node.

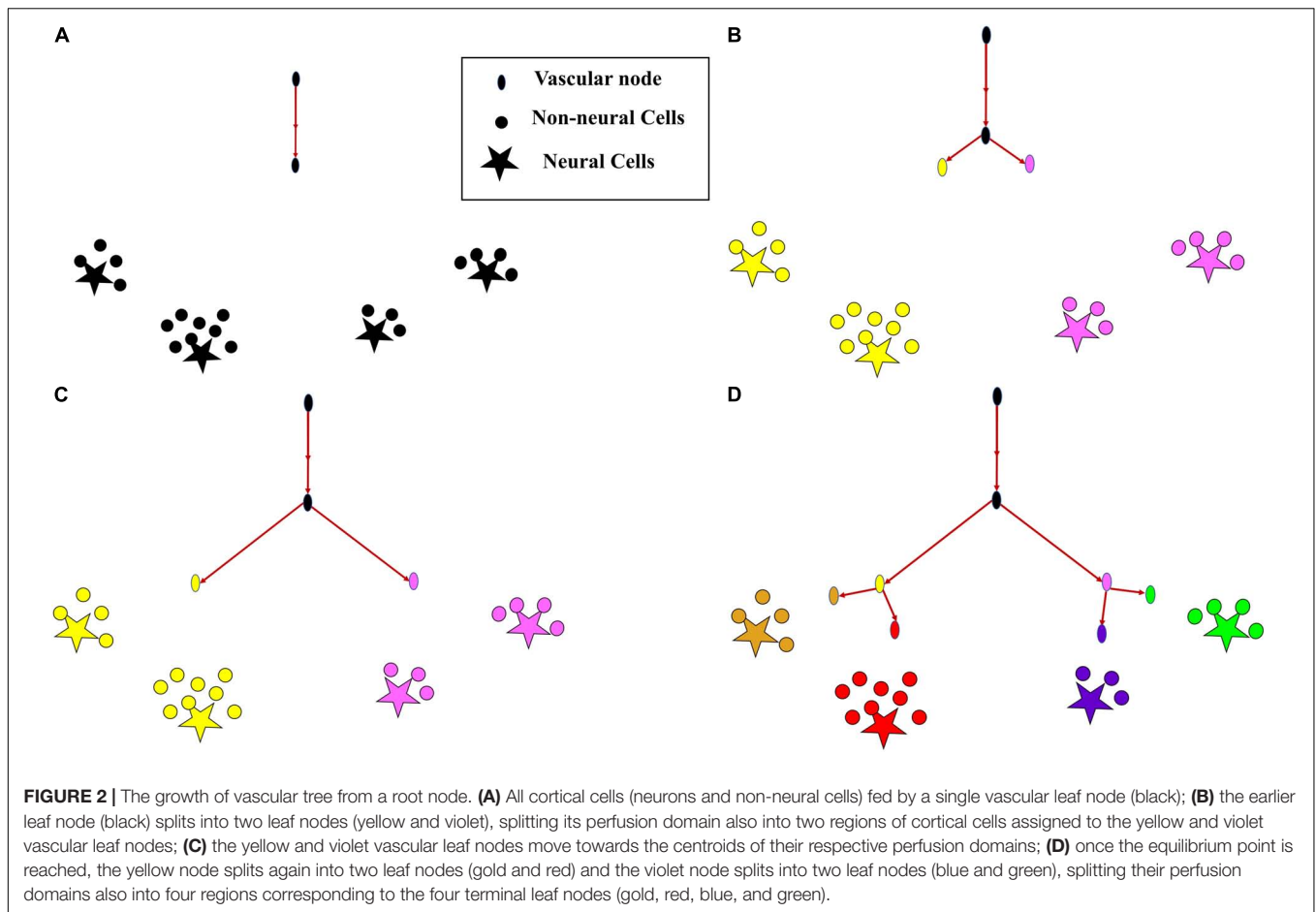
Phase II: The Settling Phase

Once the tree spans the space such that there are m leaf nodes, the settling phase begins. Here, a grown tree rearranges itself so as to optimize the cost of path length and wire length. To optimize the path and wire lengths, we try to minimize the sum

of squared pathlengths, sum of squared wirelengths and sum of squared distances from leaf nodes to tissues. The cost function to be optimized consists of three components, (i) Total squared path length (TSPL), (ii) Total squared wire length (TSWL), (iii) Total squared tissue-vascular distance (TSTD).

For a given vascular tree, let there be L number of levels. Let the level of hierarchy of any node j in the vascular tree be denoted by l_j . The root node is identified as the top of the hierarchy with level number, $l_j = 1$. Let the level number of the vascular terminal leaf nodes be $l_j = L$.

(1) Total squared path length (TSPL) minimization:



The TSPL of the vascular tree is calculated as,

$$TSPL = \frac{1}{2} \sum_{j=1}^m n_j \left| (Q_j^p - Q_j) \right|^2 \quad (5)$$

where m is the total number of nodes in vascular tree, Q_j^p is the position of the parent node j , Q_j is the position of the j th node, n_j is the number of leaf nodes downstream the node j (**Figure 1B**). The Q_j are updated by performing gradient descent on TSPL as follows,

$$\Delta Q_j = -\eta_{path} \nabla_{Q_j} (TSPL) \quad (6)$$

(2) Total Squared Wirelength (TSWL) minimization:

The TSWL of the vascular tree is calculated as

$$TSWL = \frac{1}{2} \sum_{j=1}^m \left| (Q_j^p - Q_j) \right|^2 \quad (7)$$

where m is the total number of nodes in vascular tree, Q_j^p is the position of the parent node j , Q_j is the position of the j th node. The Q_j are updated by performing gradient descent on TSWL as follows,

$$\Delta Q_j = -\eta_{wire} \nabla_{Q_j} (TSWL) \quad (8)$$

(3) Total squared tissue-vascular distance (TSTD) minimization:

Total squared tissue-vascular distance estimates the total squared distance between the vascular nodes and the cortical cells assigned to them. The distance between a vascular leaf node j ($j \in LN$), and the cortical cells ($P_i, i \in C_j$), where C_j denotes the set of cortical cells assigned to the vascular leaf node j , is given by

$$D_j = \frac{1}{2} \sum_{i \in C_j} \|P_i - Q_{j(i)}\|^2 \quad (9)$$

The TSTD is calculated as

$$TSTD = \sum_{j \in LN} D_j \quad (10)$$

where LN denotes the set of leaf nodes. Note that the expressions on the right-hand side in eqs. (9,10) are the same as those in eqs. (1,2) respectively.

The Q_j 's are updated by performing gradient descent on TSTD as follows,

$$\Delta Q_j = -\eta_{tiss} \nabla_{Q_j} (TSTD) \quad (11)$$

Jointly, eqs. (6, 8, 11), govern the settling process, which continues until the vascular tree converges. Convergence

criterion is given by, $\zeta \rightarrow 0$, where ζ is defined as,

$$\zeta = \frac{1}{m} \sum_{j=1}^m ||Q_j(t+1) - Q_j(t)||^2 \quad (12)$$

Estimation of the Length of Vessels. The length of a vessel formed by connecting a parent node x to a child node y , is defined as the Euclidean distance between the parent node (x) and the child node (y).

$$\zeta_{y,x} = |\vec{x} - \vec{y}| \quad (13)$$

Since we estimate the volume density in each layer, the length contribution of each vessel in each layer is identified by measuring its length inside the specified layer.

Estimation of the Vessel Radius

The radius of each vessel is defined based on its level of hierarchy in the vascular tree. The radius at each level is iteratively fit in such a way so as to obtain the volume density distribution as close as possible to experimentally observed values. Two steps of iteration are followed. First, the microvessel radii are approximated to fit the microvascular volume density observed experimentally. Then, after fixing the microvascular radii, the radii of the higher levels are estimated such that the total vascular volume density is closest to the experimental observation. All radii below $3 \mu m$ were considered to be microvessels. The level at which the vessels become microvessels was considered as a free parameter.

The radius of the vessels at each level of hierarchy in the vascular tree was arranged as an array (R) of dimension $L \times 1$ (L is the number of levels) and was initialized as $R = R_0$. The vascular volume density from the model (\widehat{V}_λ) is estimated based on the value of R . The desired output (V_λ) is the value of the vascular volume density at each layer λ , as obtained from the experiment (Tsai et al., 2009). The cost function (C) is defined by the mean squared error between V_λ and \widehat{V}_λ .

$$C = ||V_\lambda - \widehat{V}_\lambda||^2 \quad (14)$$

The radius of a randomly chosen level was increased by a small value ΔR such that C decreased continuously. Once an update is made to radii of all levels, the radii were adjusted to make sure that they follow a descending order of magnitude from root node level to leaf node level. The iterations were carried out until the magnitude of C was less than 10^{-9} .

The approximation was also carried out using linear regression. The cost function was calculated for each layer (λ). In each layer the vessels were identified based on their level of hierarchy in the vascular tree, and a radius was assigned to each of them (r_λ^φ) accordingly. The length contribution of each vessel to that layer was also calculated (ξ_λ^φ) using trigonometric principles (please see **Supplementary Material Section S1** for detailed explanation). The cost function per layer is defined by

$$C_\lambda = \left| V_\lambda - \frac{\sum_{\varphi=1}^L \pi (r_\lambda^\varphi)^2 \xi_\lambda^\varphi}{v_\lambda} \right|^2 \quad (15)$$

where $v_\lambda = \text{Length} \times \text{Width} \times \text{Height}$ of the volume of an individual layer. Note that in eq. 15, we use the formula for the

volume of a cylinder $\pi r^2 l$, where r is the radius and l the length of the cylinder.

The gradient of the radii of vessels at each level of hierarchy in the vascular tree was calculated such as to minimize the cost function (C_λ)

$$\Delta r_\lambda^\varphi = -\eta_r (V_\lambda - \widehat{V}_\lambda) (-2\pi) r_\lambda^\varphi \xi_\lambda^\varphi \quad (16)$$

The iteration was looped over the total number of layers and the entire iteration was repeated until C was less than 10^{-9} .

But since we consider stacked layers instead of sliding layers with overlap, both the above methods were only able to yield a crude approximation.

Estimation of Volume Density in Each Layer

Once the optimal values of radii for each layer were obtained, the vascular volume density (\widehat{V}_λ) was calculated for each layer using the equation below.

$$\widehat{V}_\lambda = \frac{\sum_{\varphi=1}^L \pi (r_\lambda^\varphi)^2 \xi_\lambda^\varphi}{v_\lambda} \quad (17)$$

The microvascular volume density ($\widehat{V}_{\mu\lambda}$) was calculated by considering the microvessels only (vessels whose radii is less than or equal to $3 \mu m$).

$$\widehat{V}_{\mu\lambda} = \frac{\sum_{\varphi \in L_\mu} \pi (r_\lambda^\varphi)^2 \xi_\lambda^\varphi}{v_\lambda}, r(\lambda) \leq 3 \mu m \quad (18)$$

where L_μ indicates the level of hierarchy in the vascular tree beyond which the vessel radii are less than or equal to $3 \mu m$.

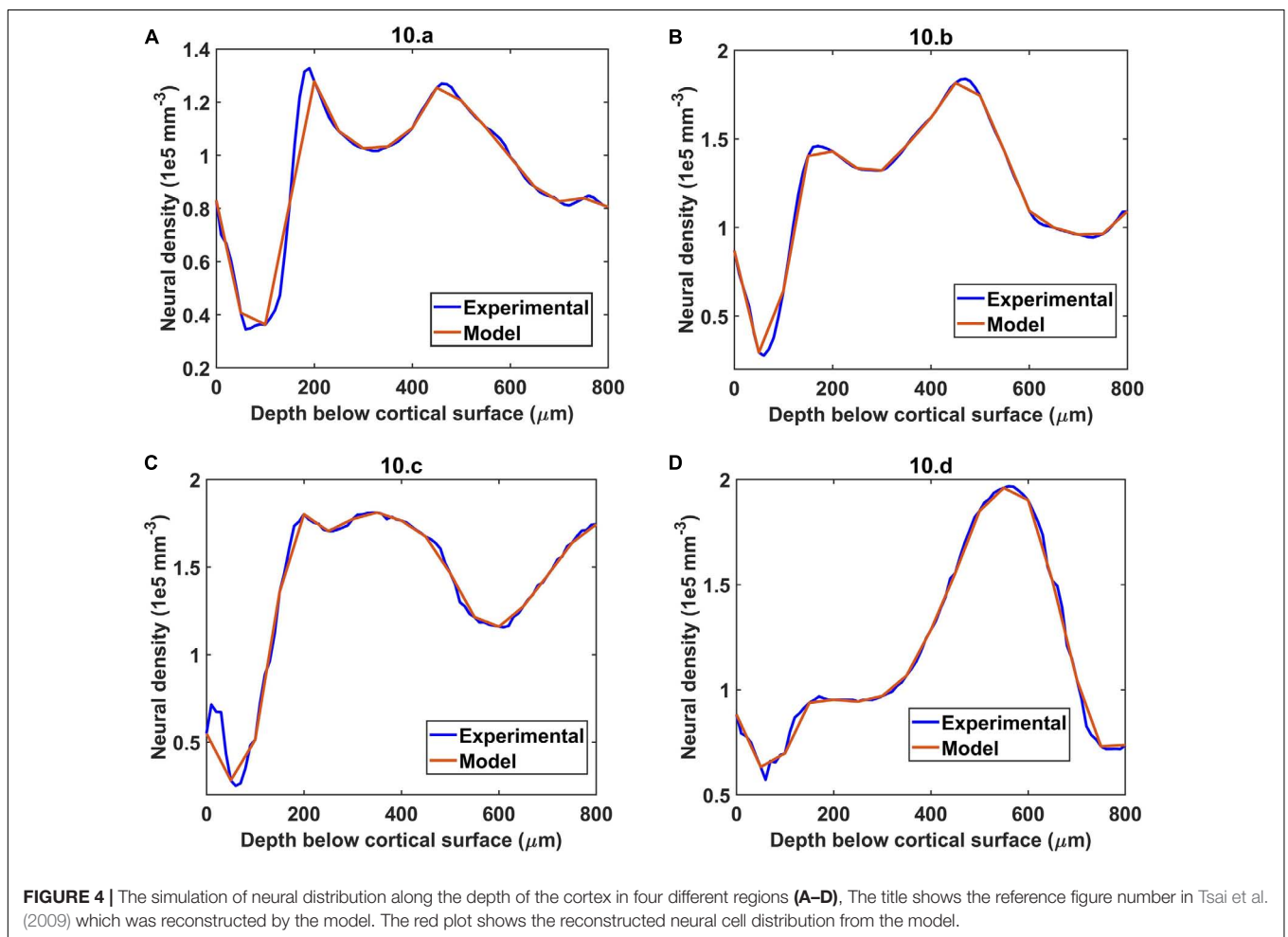
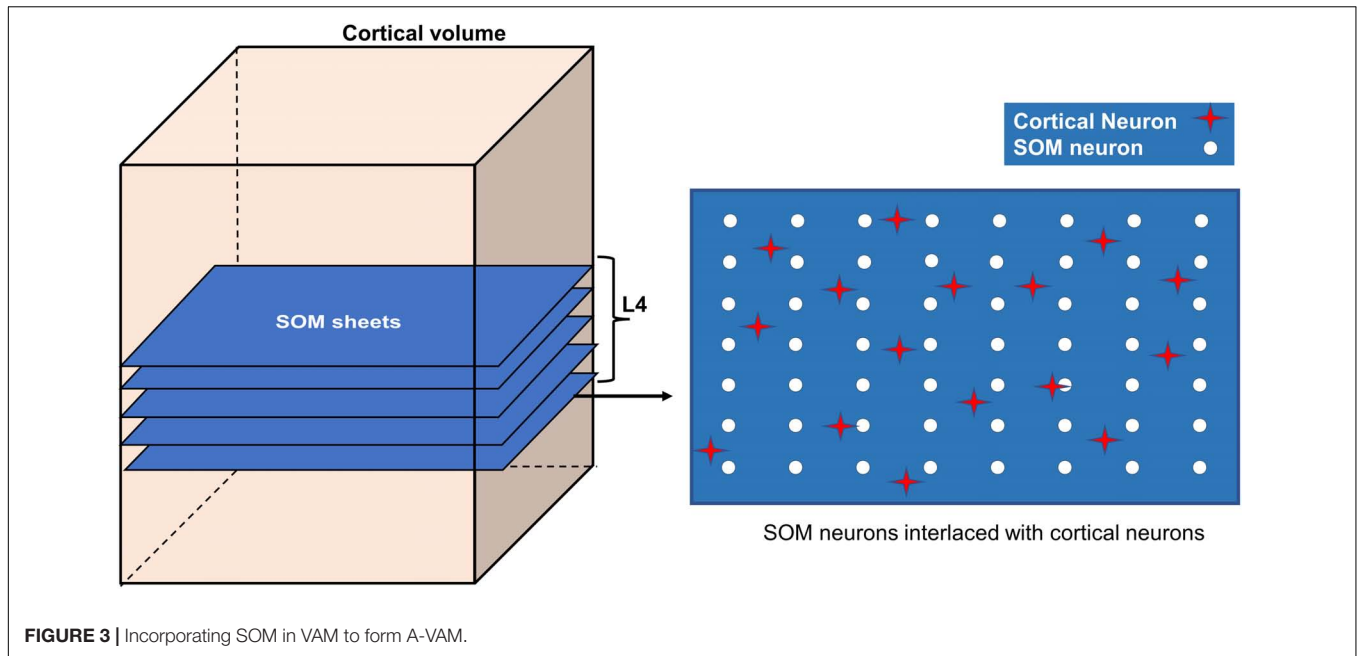
Estimation of Mean Distance Between Vessels and Neurons

The distance between a neuron at coordinate P_i and its closest vessel at coordinate $Q_{j(i)}$ was estimated for all neurons in λ 'th layer. The mean squared distance (D_λ) in that layer was defined as the average of squared Euclidean distance between all neurons in that layer and their respective closest vascular leaf node. Let the set S_λ denote the indices of the neurons which belong to layer λ .

$$D_\lambda^2 = \frac{\sum_{i \in S_\lambda} ||P_i - Q_{j(i)}||^2}{n_\lambda} \quad (19)$$

Vascular Arborization Based on Neural Activity and Neural Cytoarchitecture

In the first part of the VAM simulation study, we simulated a small volume in the somatosensory cortex ($100 \mu m \times 100 \mu m \times 800 \mu m$). The model was able to grow a vascular tree true to the experimental observations. Hence, we expand the model to a larger volume spanning a volume of ($600 \mu m \times 600 \mu m \times 700 \mu m$). The number of root nodes in this larger volume was estimated to be ~ 44 as per the experimental observations by Wu et al. (2016). The root nodes were fixed randomly from a Gaussian distribution. The VAM model was modified so as to incorporate the influence of neural activity in addition to neural and non-neural cytoarchitecture on the vascular tree growth. The modified VAM model is called the Activity-based Vascular Arborization Model (A-VAM).



Two types of metrics are used to compare the A-VAM simulations with the experiments: (a) Branch Point Density (BPD), and (b) Vascular Length Density (VLD). The BPD is defined as the density of the vascular nodes in a given volume. Given that in a tissue volume (ψ) with length a , width b , and height c , the total number of vascular nodes counts to m_ψ

$$BPD = \frac{m_\psi}{\psi} \quad (20)$$

where $\psi = abc$, is the total volume of the tissue under consideration.

The Vascular Length Density (VLD) is defined as the ratio of the cumulative length (α_ψ) of all the vessels in the volume to the volume of the tissue.

$$VLD = \frac{\sum_\psi \alpha_\psi}{\psi} \quad (21)$$

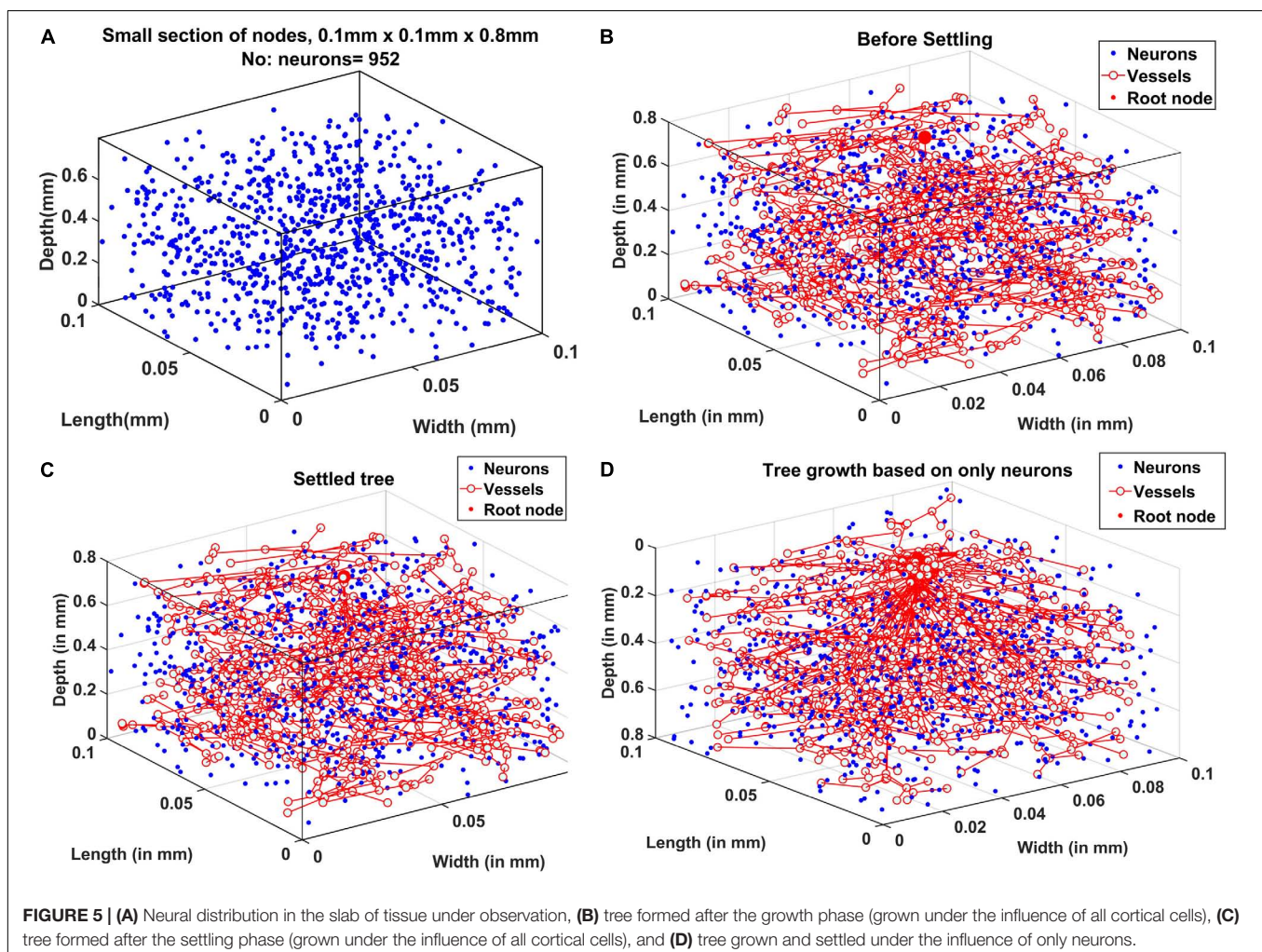
In A-VAM, there are three major stages for the tree growth (i) Prenatal growth phase, (ii) Post-natal growth phase, and (iii) Settling Phase.

Prenatal Growth Phase

This phase simulates the vascular arborization which occurs during fetal development until the birth. Here we assume that there is minimal to nil neural activity and hence the vascular arborization completely depends on the neural cytoarchitecture. We run the prenatal growth phase to ensure that the BPD and VLD are close to experimentally observed values at birth.

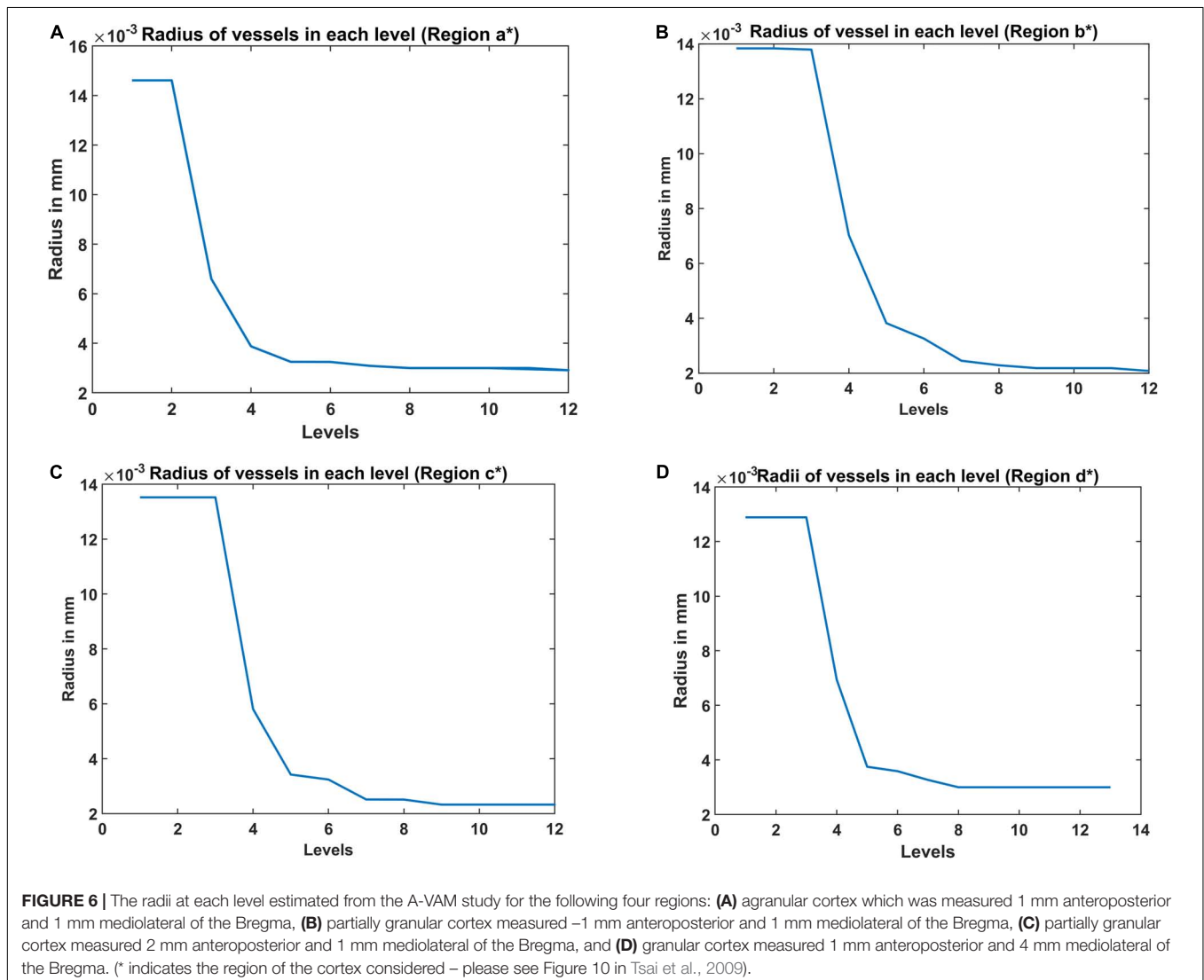
Post-natal Growth Phase

During post-natal phase, we assume that the vascular arborization depends on neural activity in addition to neural cytoarchitecture. The neural network is simulated using a Self-Organizing Map (SOM) which results in a topographic mapping of input (Kohonen, 1990). The SOM model is trained using input stimuli curated to imitate the whisker simulations. Each whisker simulation is represented as a two-dimensional Gaussian distribution centered around the pixel representing the whisker under simulation. The afferent weight connections of the winning neuron and its neighbors are moved closer to the input vector scaled by a Gaussian function which peaks at the winning neuron (please see **Supplementary Material 2** for details of SOM training).



The different layers of somatosensory cortex in rodents produce different responses to whisker stimulation. Layer 4 (L4) region is known to show the earliest and fastest response to whisker stimulation (Woolsey et al., 1996; Vanzetta et al., 2004; Wu et al., 2016). Whisker stimulations are represented topographically in the form of barrels (whisker barrels) in L4. In addition to the whisker identification and mapping in layer 4, other layers of the somatosensory cortex like the layer 2/3 (L2/3) are capable of mapping the additional features of whisker stimulation like the orientation (Lee et al., 2005; Kremer et al., 2011; Kwon et al., 2018). In the current study, we explore the influence of neural activity on vascular arborization, specifically in L4. The whisker stimulations given to the VAM model are modeled using spatially distributed two-dimensional isotropic Gaussian input which has no orientation information. The neural map formed by training a single layer self-organization map (SOM) using the isotropic Gaussian inputs can represent the barrel maps formed in L4. To observe the influence of neural activity on vascular arborization in other layers, for

example, L2/3, the SOM needs to have an additional layer that represents the L2/3. The orientation mapping observed in L2/3 can be attained in the current model by including a second layer of SOM which receives input from the primary SOM representing L4 activity, and by training the updated network of SOMs with appropriate oriented bar stimuli in place of the isotropic Gaussian input. The updated SOM network can be added to VAM by incorporating the second layer of SOM in the L2/3 region. However, since the objective of the study requires only the L4 activity, to maintain the simplicity of the model, we introduce the neural activity only in L4 (the region between depth 0.3 mm to 0.5 mm from the surface). Hence in the model, we introduce the neural activity only in L4 (the region between depth 0.3 mm to 0.5 mm from the surface). The SOM layer is stacked up in this volume as shown in **Figure 3**. The neural units in the SOM are distributed uniformly in each layer as shown in the right panel in **Figure 3** (white circles). The activity (δ_i) of each *i*th cortical neuron (red star in **Figure 3**, right panel) depends on the activity of the



nearest SOM neuron (Z_i) and its distance (ϑ) from the SOM neuron as follows.

$$\delta_i = Z_i * e^{-\vartheta^2} \tag{22}$$

The vascular tree growth equation was modified such that the neural activity (δ_i) also influences the learning rate of the growth and arborization of the vessels.

While incorporating the effect of neural activity in the growth phase, the learning rate, η_g , varies for each neural tissue based on its activity. The learning rate (η_{g_i}) at which each i th neuron influences the calculation of gradient ΔQ_j of the j th vascular node is given by

$$\eta_{g_i} = k_1 \eta_g + k_2 \delta_i \tag{23}$$

where k_1 and k_2 are constants and $i \in C_j$.

An additional constraint was also introduced to make the stopping criteria also depend on the neural demand. In order for

a vascular node to split and give rise to child nodes, the perfusion domain of the vascular node should have a minimum neural activity (δ_{min}) in addition to the requirement of $\Delta Q_j \approx 0$. If a node j has a very small gradient ($\Delta Q_j \approx 0$) but does not have the minimum neural activity in its perfusion domain, then that node is declared as a leaf node. The vascular network grows until all the nodes are labeled as terminal nodes.

The Settling Phase

The settling phase starts once the tree is grown completely. Similar to the settling phase in VAM, in A-VAM also, fully grown trees undergo settling under the influence of neural activity in addition to tissue cytoarchitecture. The learning rate (η_{tiss}), used while calculating the gradient ΔQ_j using the TSTD, would depend on the neural activity as follows:

$$\eta_{tiss}(i) = k_3 \eta_{tiss} + k_4 \delta_i \tag{24}$$

where $i \in C_j$.

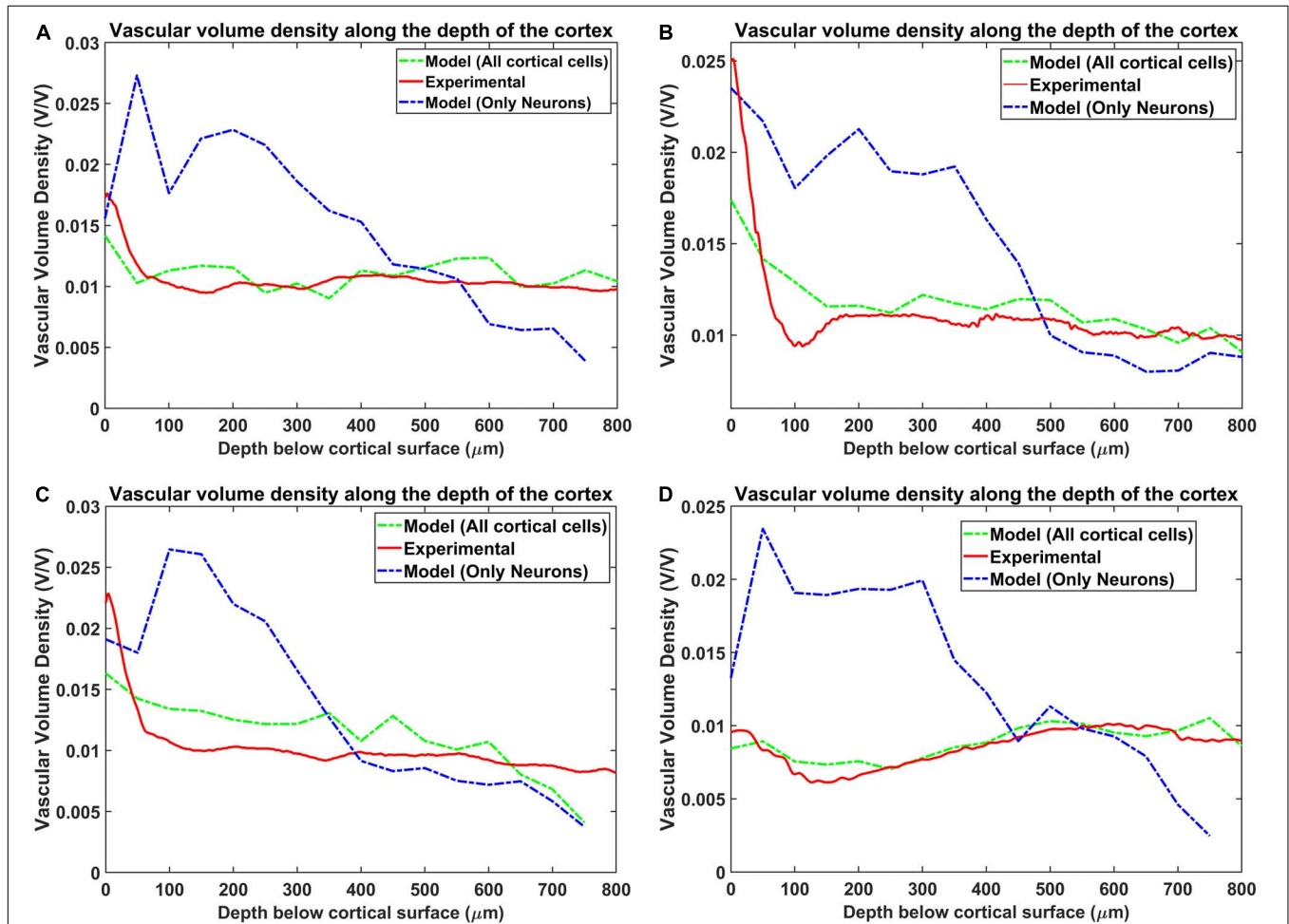


FIGURE 7 | Comparison of the vascular volume density from all the four regions when considering neurons alone and both neurons and non-neural cells. The four regions are (A) agranular cortex which was measured 1 mm anteroposterior and 1 mm mediolateral of the Bregma, (B) partially granular cortex measured -1 mm anteroposterior and 1 mm mediolateral of the Bregma, (C) partially granular cortex measured 2 mm anteroposterior and 1 mm mediolateral of the Bregma, and (D) granular cortex measured 1 mm anteroposterior and 4 mm mediolateral of the Bregma. The experimental data is from Tsai et al. (2009).

Table of parameters and constants

η_g	5×10^{-5}
δ_{min}	0.07
$\eta_{path}(prenatal)$	1.7×10^{-4}
$\eta_{wire}(prenatal)$	1.15×10^{-4}
$\eta_{tiss}(prenatal)$	2.5×10^{-4}
$\eta_{path}(postnatal)$	1.8×10^{-4}
$\eta_{wire}(postnatal)$	1.5×10^{-4}
$\eta_{tiss}(postnatal)$	2×10^{-4}
k_1	0.1
k_2	1×10^{-4}
k_3	1
k_4	9×10^{-5}

RESULTS

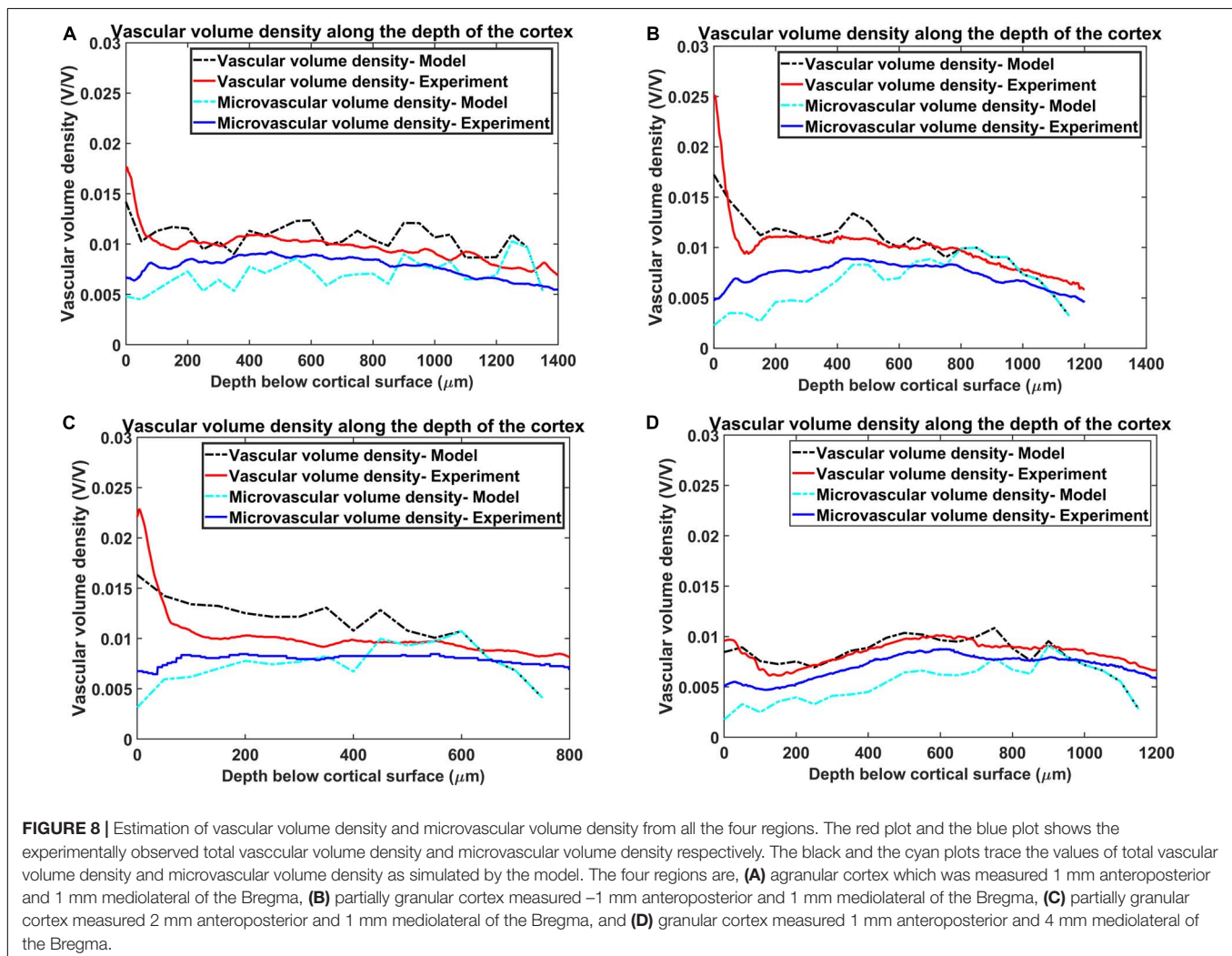
Distribution of Neurons

The neural distribution was simulated for four different regions considered in the experiment by Tsai et al. (2009). The four

regions were: (a) agranular cortex which was measured 1 mm anteroposterior and 1 mm mediolateral of the Bregma, (b) Partially granular cortex measured -1 mm anteroposterior and 1 mm mediolateral of the Bregma, (c) Partially granular cortex measured 2 mm anteroposterior and 1 mm mediolateral of the Bregma, and (d) Granular cortex measured 1 mm anteroposterior and 4 mm mediolateral of the Bregma. The model assumed 16 layers of $50 \mu\text{m}$ height stacked one on top of another and sampled the neural cell density at each $50 \mu\text{m}$ depth to reconstruct a similar neural distribution. The reconstructed neural cell number density is shown by the red plots in **Figures 4A–D**. The experimental values were obtained from the Figure 10 of Tsai et al. (2009).

Vascular Tree Growth

An example of neural distribution inside a slab of dimension $0.1 \text{ mm} \times 0.1 \text{ mm} \times 0.8 \text{ mm}$ is shown in **Figure 5A**. The vascular node was initialized at the center of the cortical surface as shown by the larger red sphere in **Figure 5B**. **Figure 5C** shows the tree after the settling phase. Even though the difference in



tree structure is not evident by a comparison of **Figures 5B** and **5C**, settling phase brings in fine adjustments in the tree which is evident clearly in the comparison of vascular volume density comparison.

The tree growth phase was tried using two conditions – the first one by assuming that the tree growth would be influenced by cytoarchitecture of neurons only. The tree grown based on this assumption is shown in **Figure 5D**. The alternate assumption was that not only neurons but non-neural cells also influence the tree growth. The grown tree in **Figures 5B,C** was based on this assumption. In both **Figures 5B,C** and **5D**, the number of vascular leaf nodes were fixed to be equal to 70% of the total number of non-neurons. This was to ensure that in both the assumptions, the number of leaf nodes are equal.

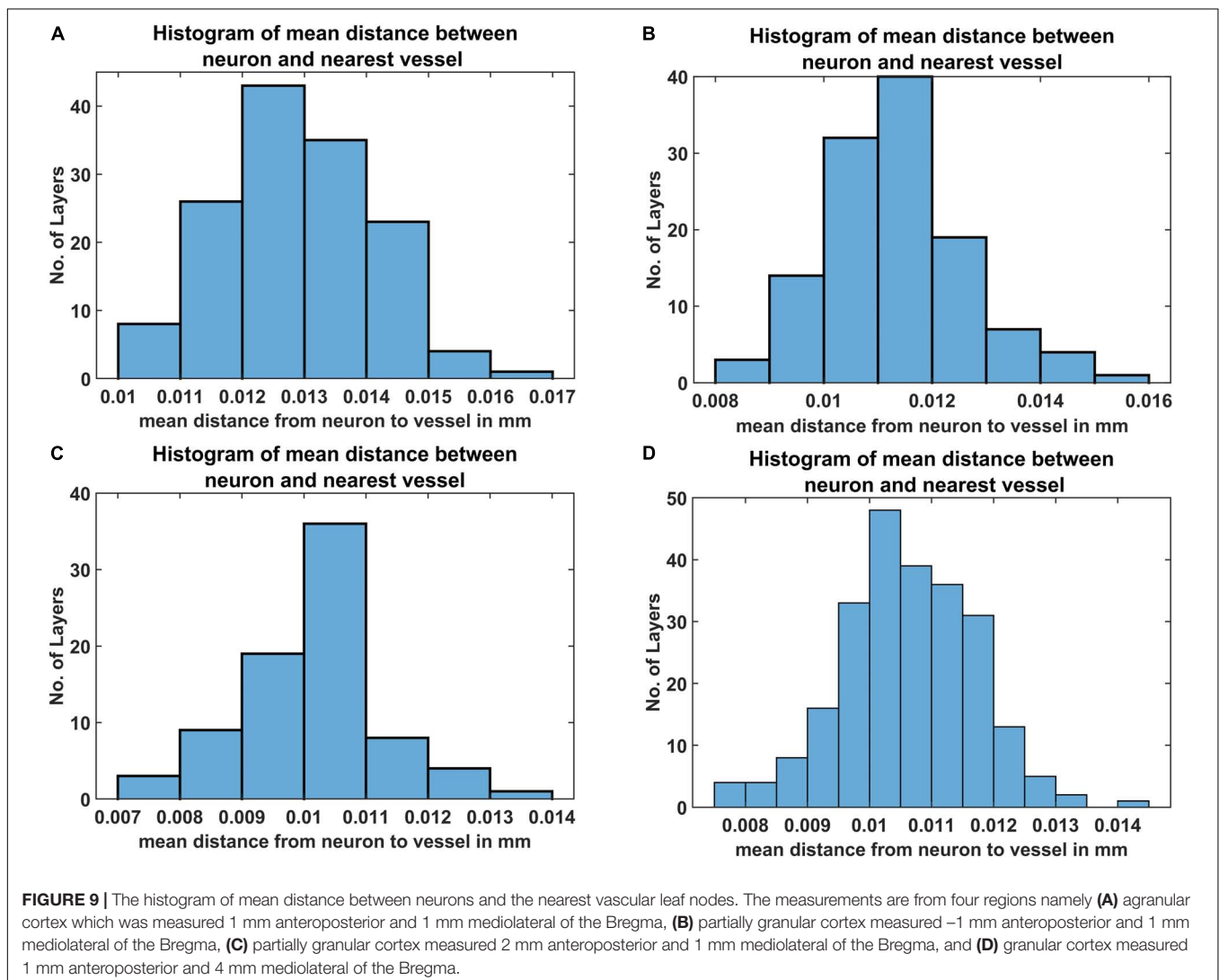
Radius of the Vessel at Each Level in Vascular Tree Hierarchy

The radius of the vessel at each level was iteratively calculated to give the best approximation of the experimentally observed

vascular volume density of the vessels (**Figure 6**). The range of radii are in agreement with the range of arteriolar diameter observed experimentally in rats and mice (Zhang et al., 2014; Lugo-Hernandez et al., 2017). The maximum diameter of the blood vessel was 30 μm . The radius decreases at each level of the bifurcation until the vessel is declared a terminal leaf node which is analogous to the capillaries whose diameter is close to 4 μm (radius $\sim 2 \mu\text{m}$) agreeing with experimental observations (Coelho-Santos and Shih, 2020).

Vascular Volume Density

The vascular volume density was calculated at each layer of dimension 0.1 mm \times 0.1 mm \times 0.05 mm. The vessels in each layer were identified and the volume contribution was calculated based on its length in the layer and the level of the vessel. The **Figures 7A–D** compare the reconstructed vascular volume density in the four regions of the cortex. The vasculature was grown using two methods: (i) only neurons influence the vascular growth, and (ii) both the neurons and the non-neurons influence



the vascular growth. As can be observed from the plot, the green dashed line shows the vascular volume density estimated from the settled tree grown using all the cells, the neurons and the non-neural cells. The blue dashed line on the other hand is the vascular volume density obtained from the tree grown using only neurons. We can observe that the estimation from the tree grown using all the cells is a better approximation than from the model grown based on only the neurons. This suggests that the cytoarchitecture of both neurons and non-neural cells plays an important role in deciding the vascular architecture.

The **Figures 8A–D** show the reconstructed microvascular volume density and the total vascular volume density in comparison with the experimental values. We defined the vessels of radii less than $3\ \mu\text{m}$ (Tsai et al., 2009) (all the vessels below level 7) as part of microvasculature. The similarity of the model with the experiment shows that the radii distribution along the levels and vascular architecture is a reasonable approximation of the biologically observed vasculature.

Mean Distance Between Vessels and Neurons

The mean distance between vessels and neurons was estimated for each layer as per eq. (19) and the distribution was depicted as a histogram. **Figures 9A–D** shows the histogram of mean distance between neurons and the closest vessel calculated across the layer. It was observed that in all the four cases, the mean value is between 0.010 mm and 0.013 mm, which is close to 0.014mm, the biologically observed value as shown in Figure 9C of Tsai et al. (2009).

The Correlation Between Neural Areal Density and Vascular Volume Density

Direct visual inspection of the neural density distribution (**Figure 4**) and vascular density distribution (**Figures 7, 8**) suggests that the neural density does not covary with the vascular

density, agreeing with experimental studies. To confirm this inference, the average Pearson correlation coefficient was also estimated and found to be less than 0.2. We then checked if the model was able to show the correlation which exists between neural areal density and microvascular density when compared over a global scale (across species and regions). We simulated the interspecies variation by choosing the number of vascular leaf terminals randomly between 35 and 45% of total neurons for each trial. Along with this, the random distribution of the neural terminals inside each layer also provided randomness. We collected data from 25 simulations in total for the four regions, and used the combined data to analyze the correlation. The neural areal density was calculated as the density of the neurons in the region under consideration multiplied by the depth of the region. As observed in experimental study by Tsai et al. (2009), we saw that the model also predicts a correlation of 0.61. The scatter plot between neural areal density and microvascular volume density across different animal models and regions is shown in **Figure 10**.

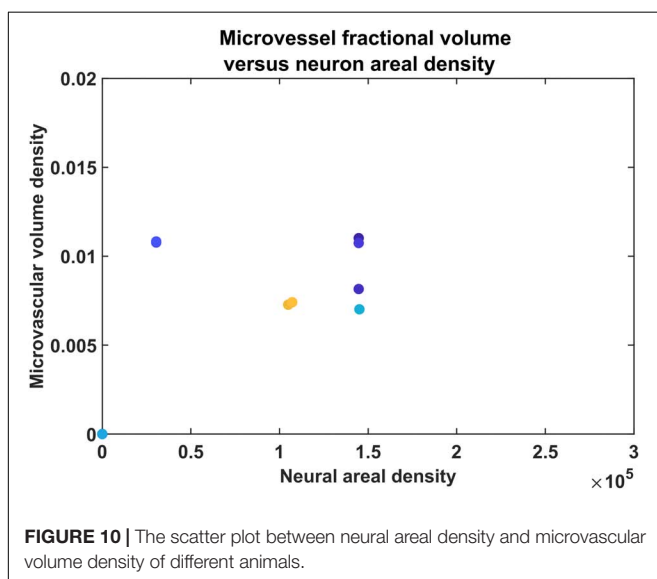
Influence of Neural Activity on Vascular Arborization

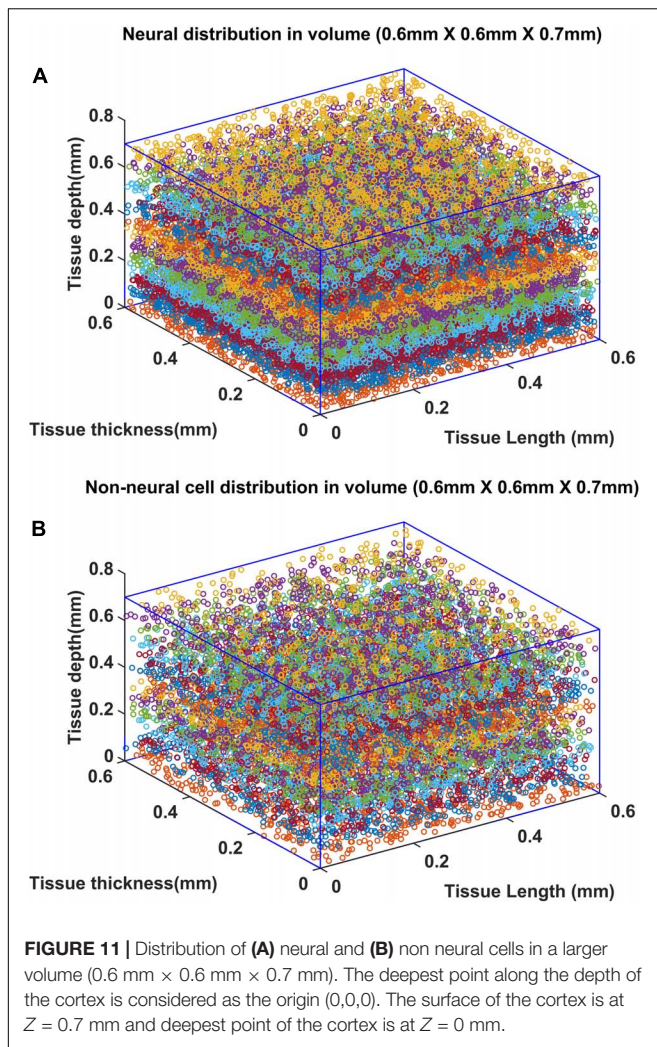
Once the VAM study established the influence of the cytoarchitecture of neural and non-neural cells on vascular arborization, we explored whether neural activity could also influence the arborization of vessels. We modified the VAM to the A-VAM to incorporate the neural activity. In order to consider the influence of neural activity on vascular arborization, a larger area of cortical tissue needs to be considered (spanning multiple barrels in the whisker barrel cortex). The vascular arborization in a larger area ($0.6\ \text{mm} \times 0.6\ \text{mm} \times 0.7\ \text{mm}$) was hence considered to model A-VAM. The neural and non-neural cells were distributed similar to the VAM implementation as shown in **Figure 11**.

Since a larger area was considered in this case, the vascular growth was initialized by defining 44 root nodes (Wu et al., 2016) distributed over the surface of the cortical tissue volume. The vascular arborization begins in the prenatal growth phase where the vascular growth depends only on the cytoarchitecture of the tissues until birth. The arborization at birth in a small volume (L4 region, between 0.3 and 0.55 mm; Wu et al., 2016) is as shown in **Figures 12A,B**. The quantified observations in terms of BPD and VLD were similar to experimental observations (**Figures 12 C,D**).

At P0, the neural activity is incorporated by means of connecting a SOM network to the VAM (**Figure 3**) making it the A-VAM. The SOM was trained for the entire whisker barrel cortex as shown in **Figure 13A**. Each colored blob represents one barrel and its activity corresponds to the activity of the whisker which it represents. The SOM interpixel distance was defined true to the biological whisker barrel dimensions (Lacoste et al., 2014). An area of $0.6\ \text{mm} \times 0.6\ \text{mm}$ was chosen (**Figure 13B**) which contained three barrels each of B, C and D row whiskers (Enclosed by red square in **Figure 13B**) for incorporating with the VAM.

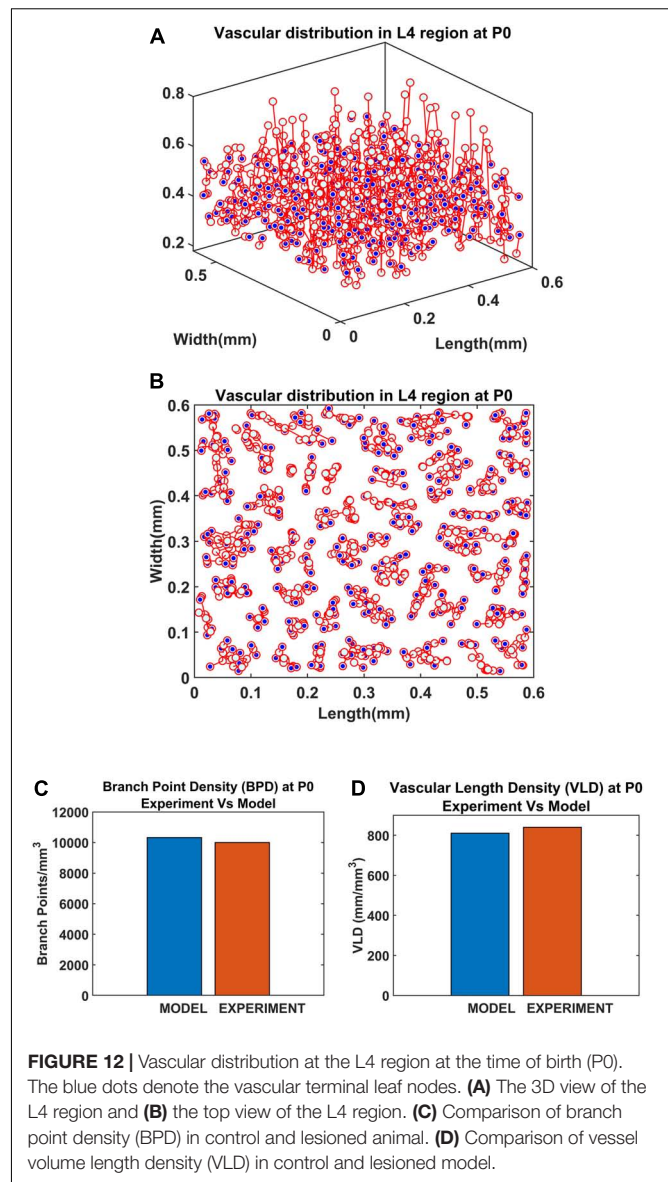
The selected area of SOM network was stacked on the L4 area. The neural activity of each cortical neuron was estimated based on the activity of the nearest SOM neuron, and based on how far





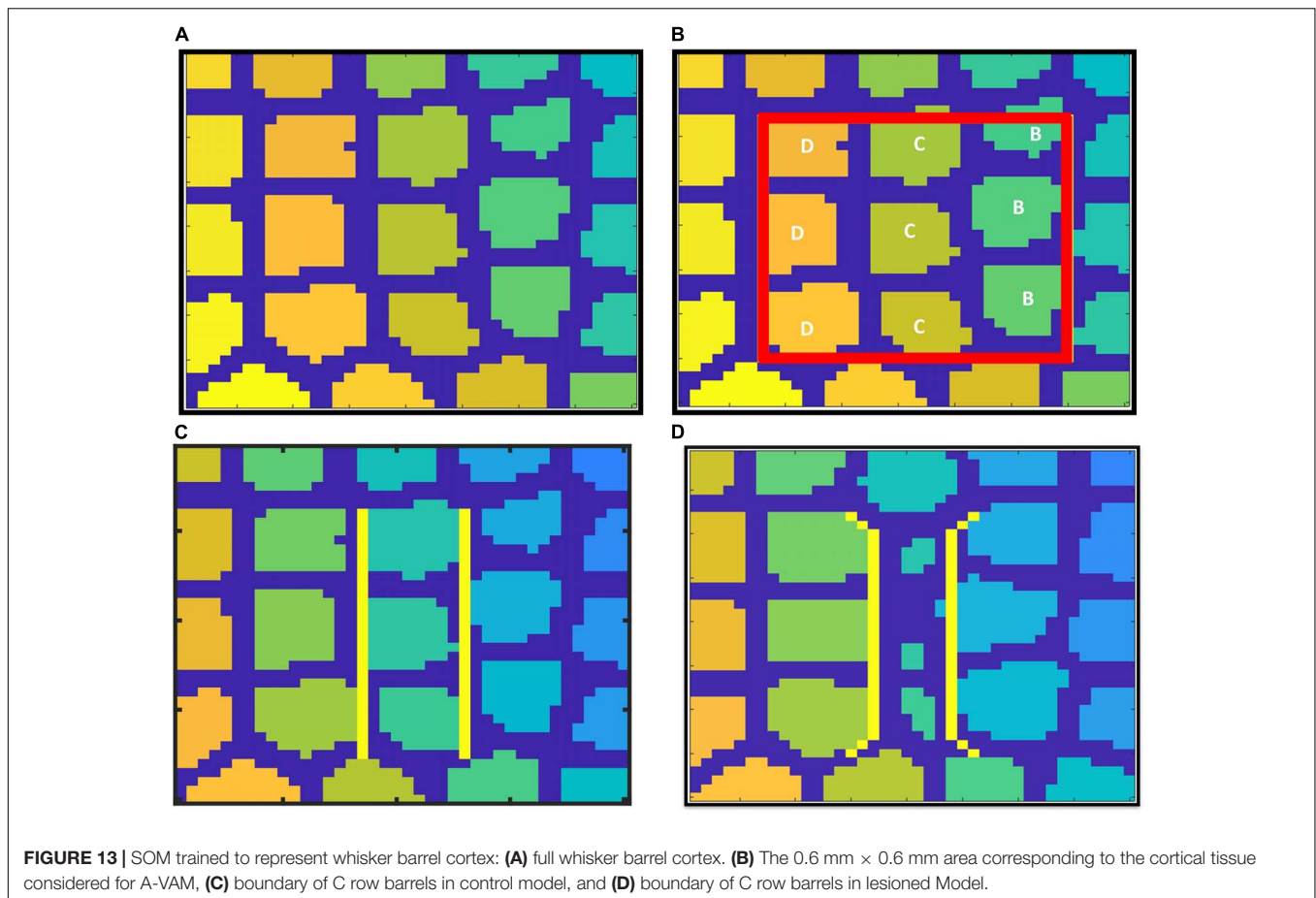
the cortical neuron is from that nearest SOM neuron. The weights of SOM during various stages of training were saved and the output of the SOM was systematically presented to the A-VAM network at every 25th iteration. We adopted such a method to ensure simultaneous learning in neural and vascular network without much computational load. Since vascular feedback to neurons is not incorporated in the current model, such an approach can be justified.

The neural activity dependent vascular arborization was explored under two criteria: (a) Control – where all the nine whiskers in the selected region were intact; (b) Lesioned – where the middle row (C row) whiskers were lesioned. In the control model, all the whiskers are represented by approximately the same area in the SOM as shown in **Figure 13C**. In the lesioned model, the representation of whiskers in the trained SOM network look like in **Figure 13D**. The area representing the lesioned middle row (C row) shrinks while the neighboring rows (B and D) are represented by a larger area. With the help of A-VAM, we explore how such a change would affect the vascular arborization. The yellow lines in both **Figures 13C** and **13D**



mark the boundary of the C row considered to evaluate the vascular density.

The vasculature was allowed to grow, and span the tissue region until the tree converges (until all growing vascular nodes are declared as terminal leaf nodes). The settled vascular tree in the L4 region of the control and lesioned cases were as observed in **Figures 14A,B**. The top views of the 3D plots are shown in **Figures 14C,D**. The blue dots represent the vascular leaf nodes. By visual inspection of the top views of the L4 region (**Figures 14C,D**), we can see that there is a reduction in branch point density in the lesioned model when compared with the control model. To get a more quantitative account of the difference, we calculated the BPD and VLD of both the models at the L4 volume in the area between the yellow lines marked in **Figures 13C,D**. The resulting values showed that the BPD and VLD of the lesioned model was significantly lesser when



compared to the control model (**Figures 14E,F**), as observed by the experimental study. This concludes that the neural activity along with the cytoarchitecture of neural and non-neural cells influences vascular arborization.

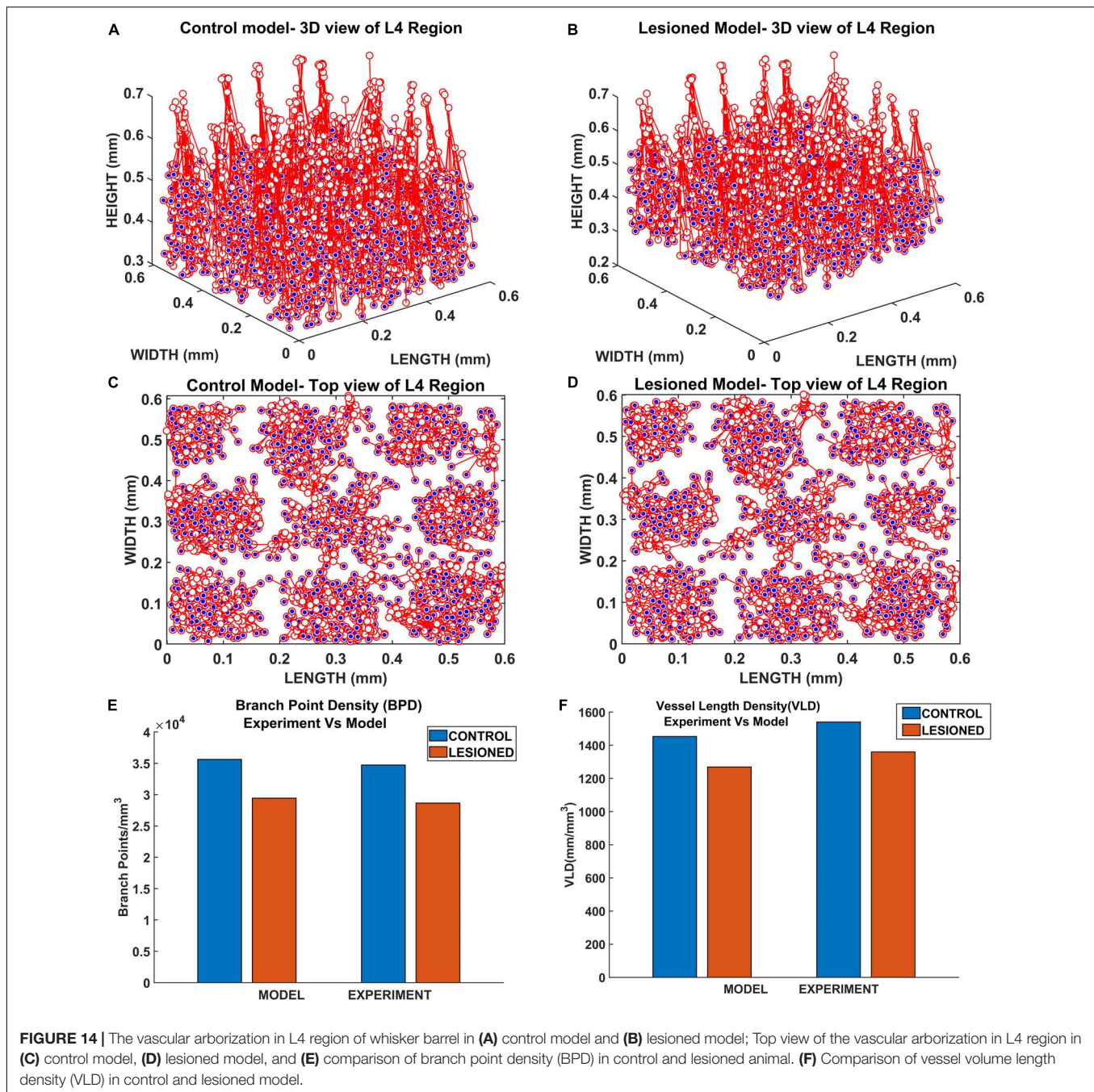
DISCUSSION

Our first model of vascular tree growth, VAM, which was based purely on the cytoarchitecture of the cortical cells was able to simulate a fully grown vascular network from a single root node. VAM model showed that the vascular arborization is influenced by the cytoarchitecture of neurons as well as the non-neural cells such as the glial cells. The model resulted in a vascular tree that closely approximates the experimental vascular tree as characterized by several indices. The microvascular volume density and the total vascular volume density estimated from the model were in close agreement with the experimental studies (Tsai et al., 2009). The mean distance between vessels and neurons in the model was close to 14 μm , the biologically observed value. The model also shows that the neural densities do not covary with the vascular density along the depth of the cortex, but revealed a high correlation between neural areal density and microvascular density when compared over a global scale (across animals and regions). Moreover, the range of estimated

vessel radii that resulted in this vascular volume density agreed with the range of arteriolar diameters observed experimentally in rats and mice (Zhang et al., 2014; Lugo-Hernandez et al., 2017).

Inspired by the recent observations that the neural activity also could influence the vascular arborization, we modified the VAM to A-VAM, making the tree growth depend on the neural activity as well. The neural layer modeled using SOM network impacted the vascular tree growth in both the growth phase and settling phase. The grown tree was characterized in terms of branch point density and vascular volume density. The vascular arborization observed in control vs. lesioned models evidently showed that the branch point density and the vascular volume density are significantly lower in the latter. This was in agreement with the experiments done on mice whisker barrel cortex (Lacoste et al., 2014).

The study corroborates the statement that neurovascular coupling begins from a very early stage of growth. The development of neural and vascular networks takes place in parallel such that there is a mutual influence. The comprehensive understanding of the influence of neural activity on vascular arborization could be a game-changer in stroke rehabilitation therapy. Angiogenesis and neurogenesis post-stroke conditions are known to be mediated by a number of molecules of both neural and vascular origin



(Beck and Plate, 2009; Kanazawa et al., 2017a,b; Freitas-Andrade et al., 2020; Hatakeyama et al., 2020). Even though the relationship between angiogenesis and neurogenesis in the ischemic brain is theoretically hypothesized, it is yet to be validated. In such a scenario, a bidirectionally coupled neurovascular growth model would help to understand the significance of multiple pathways which are hypothesized to play a role in neurovascular remodeling.

The role of computation in shaping the morphological characteristics of neuronal branching was investigated by Cuntz et al. (2010) based on the computational principles that govern

neuronal morphologies laid out by Ramoin y Cajal (1995). They showed that a simple growth algorithm that optimizes the total cable length and the path length from any point to the root in an iterative fashion can generate synthetic dendritic trees that are indistinguishable from their real counterparts for a wide variety of neurons.

The astrocytic arborization is relatively less explored. A recent study (Verisokin et al., 2021) modeled the astrocyte morphology by forming Voronoi partitioning around randomly distributed seed points and matching the polygonal area patch from a given Voronoi partition to the closest astrocyte template extracted from

experimental images of astrocytes. However, to the best of our knowledge, there are no published computational models that simulate the arborization of astrocyte processes.

Neurons are dependent on the continuous supply of energy substrates from the cerebral vessels, and hence their firing depends on the vascular feedback to a large extent. However, in case of the A-VAM, though it captures the neural influence on angiogenesis, the current version does not include the vascular influence on neural activity. For the initial validation, we assume a healthy vascular supply and hence the feedback to the neurons were assumed to be adequate and continuous. The integration of the blood flow dynamics becomes relevant when considering the vascular remodeling along with the arborization.

The relevance of a healthy vasculature in shaping the function of the neural network has been discussed extensively (Moore and Cao, 2008; Pradhan and Chakravarthy, 2011; Chander and Chakravarthy, 2012; Chhabria and Chakravarthy, 2016; Tourigny et al., 2019; Bright et al., 2020; Kumar et al., 2021a,b). Neurodegenerative diseases are being traced back to an impaired neurovascular functional coupling (Iadecola, 2004, 2017; Shabir et al., 2018; Ahmad et al., 2020; Muddapu et al., 2020). As opposed to the conventional view of neurons as the primary computational unit of the brain, we postulate that the neurovascular unit as a single combined unit is a more appropriate computational unit of the brain. We conclude by emphasizing that the coupling between neural and vascular networks is not limited to the functional aspects but also decides the structural development of both networks. To conclude with a poetic comment by Bautch and James (2009) – neurovascular coupling is indeed a beautiful friendship that begins in the womb and continues till the end.

SUMMARY

The A-VAM model is a computational model which proposes a method to simulate vascular arborization based on neural and non-neural cytoarchitecture and neural activity. We used two major studies to design and validate the model (Tsai et al., 2009; Lacoste et al., 2014).

The study by Tsai et al. (2009) is an experimental study that explores the distribution of neural and non-neural cells along the depth of the cortex. We used this data to simulate the cortical tissue volume where vascular arborization occurs. They also measure the vascular and microvascular volume density along the

REFERENCES

- Ahmad, A., Patel, V., Xiao, J., and Khan, M. M. (2020). The role of neurovascular system in neurodegenerative diseases. *Mol. Neurobiol.* 57, 4373–4393. doi: 10.1007/s12035-020-02023-z
- Andreone, B. J., Lacoste, B., and Gu, C. (2015). Neuronal and vascular interactions. *Annu. Rev. Neurosci.* 38, 25–46. doi: 10.1146/annurev-neuro-071714-033835
- Argandoña, E. G., and Lafuente, J. V. (1996). Effects of dark-rearing on the vascularization of the developmental rat visual cortex. *Brain Res.* 732, 43–51. doi: 10.1016/0006-8993(96)00485-4

depth of the cortex. We used this data to validate the vascular arborization carried out by the VAM algorithm. In addition, Tsai et al. (2009) investigate the mean distance of a neuron to its closest vessel and the correlation between neuronal density and microvascular volume density in within the lamina of a given region. We validated the VAM model simulations with these findings as well.

The study by Lacoste et al. (2014) is an experimental study that explored the influence of sensory-related neural activity on the structure of the vascular network. We used the study by Lacoste et al. (2014) to verify the simulations of the A-VAM model to variations in sensory input.

DATA AVAILABILITY STATEMENT

The original contributions presented in this study are included in the article/**Supplementary Material**, further inquiries can be directed to the corresponding author/s.

AUTHOR CONTRIBUTIONS

BK did the model designing, coding, analysis of the results, and manuscript preparation. SM did the model tuning, analysis of results, and manuscript preparation. SG did the model tuning and analysis of results. VC did the model designing, analysis of the results, and manuscript preparation. All authors commented on and approved the final manuscript.

ACKNOWLEDGMENTS

We thank the Department of Biotechnology (DBT), Ministry of Science and Technology, Government of India (BIO/17-18/303/DBTX/SRIN), and the Center for Complex Systems and Dynamics, IIT Madras for partial funding of this project. This manuscript was released as a Pre-print at Kumar et al. (2022).

SUPPLEMENTARY MATERIAL

The Supplementary Material for this article can be found online at: <https://www.frontiersin.org/articles/10.3389/fnins.2022.917196/full#supplementary-material>

- Argandoña, E. G., and Lafuente, J. V. (2000). Influence of visual experience deprivation on the postnatal development of the microvascular bed in layer IV of the rat visual cortex. *Brain Res.* 855, 137–142. doi: 10.1016/S0006-8993(99)02361-6
- Bautch, V. L., and James, J. M. (2009). Neurovascular development: the beginning of a beautiful friendship. *Cell Adhes. Migr.* 3, 199–204. doi: 10.4161/cam.3.2.8397
- Beck, H., and Plate, K. H. (2009). Angiogenesis after cerebral ischemia. *Acta Neuropathol.* 117, 481–496. doi: 10.1007/s00401-009-0483-6
- Behzadian, M. A., Wang, X. L., Shabraway, M., and Caldwell, R. B. (1998). Effects of hypoxia on glial cell expression of angiogenesis-regulating factors VEGF and TGF- β . *Glia* 24, 216–225.

- Bright, M. G., Whittaker, J. R., Driver, I. D., and Murphy, K. (2020). Vascular physiology drives functional brain networks. *Neuroimage* 217:116907. doi: 10.1016/j.neuroimage.2020.116907
- Carmeliet, P., and Tessier-Lavigne, M. (2005). Common mechanisms of nerve and blood vessel wiring. *Nature* 436, 193–200. doi: 10.1038/nature03875
- Chander, B. S., and Chakravarthy, V. S. (2012). A computational model of neuro-glio-vascular loop interactions. *PLoS One* 7:e48802. doi: 10.1371/journal.pone.0048802
- Chhabria, K., and Chakravarthy, V. S. (2016). Low-dimensional models of “neuro-glio-vascular unit” for describing neural dynamics under normal and energy-starved conditions. *Front. Neurol.* 7:24. doi: 10.3389/fneur.2016.00024
- Chklovskii, D. B., and Koulakov, A. A. (2004). Maps in the brain: What can we learn from them? *Annu. Rev. Neurosci.* 27, 369–392. doi: 10.1146/annurev.neuro.27.070203.144226
- Coelho-Santos, V., and Shih, A. Y. (2020). Postnatal development of cerebrovascular structure and the neuroglivascular unit. *Wiley Interdiscip. Rev. Dev. Biol.* 9:e363. doi: 10.1002/WDEV.363/FORMAT/PDF/OEBPS/PAGES/1.PAGE.XHTML
- Cuntz, H., Forstner, F., Borst, A., and Häusser, M. (2010). One rule to grow them all: a general theory of neuronal branching and its practical application. *PLoS Comput. Biol.* 6:e1000877. doi: 10.1371/journal.pcbi.1000877
- Freitas-Andrade, M., Raman-Nair, J., and Lacoste, B. (2020). Structural and functional remodeling of the brain vasculature following stroke. *Front. Physiol.* 11:948. doi: 10.3389/fphys.2020.00948
- Hatakeyama, M., Ninomiya, I., and Kanazawa, M. (2020). Angiogenesis and neuronal remodeling after ischemic stroke. *Neural Regen. Res.* 15, 16–19. doi: 10.4103/1673-5374.264442
- Hogan, K. A., Ambler, C. A., Chapman, D. L., and Bautch, V. L. (2004). The neural tube patterns vessels developmentally using the VEGF signaling pathway. *Development* 131, 1503–1513. doi: 10.1242/dev.01039
- Iadecola, C. (2004). Neurovascular regulation in the normal brain and in Alzheimer's disease. *Nat. Rev. Neurosci.* 5, 347–360. doi: 10.1038/nrn1387
- Iadecola, C. (2017). The neurovascular unit coming of age: a journey through neurovascular coupling in health and disease. *Neuron* 96, 17–42. doi: 10.1016/j.neuron.2017.07.030
- Ii, S., Kitade, H., Ishida, S., Imai, Y., Watanabe, Y., and Wada, S. (2020). Multiscale modeling of human cerebrovasculature: a hybrid approach using image-based geometry and a mathematical algorithm. *PLoS Comput. Biol.* 16:e1007943. doi: 10.1371/journal.pcbi.1007943
- James, J. M., Gewolb, C., and Bautch, V. L. (2009). Neurovascular development uses VEGF-A signaling to regulate blood vessel ingress into the neural tube. *Development* 136, 833–841. doi: 10.1242/dev.028845
- Kanazawa, M., Miura, M., Toriyabe, M., Koyama, M., Hatakeyama, M., Ishikawa, M., et al. (2017a). Microglia preconditioned by oxygen-glucose deprivation promote functional recovery in ischemic rats. *Sci. Rep.* 7:42582. doi: 10.1038/srep42582
- Kanazawa, M., Ninomiya, I., Hatakeyama, M., Takahashi, T., and Shimohata, T. (2017b). Microglia and monocytes/macrophages polarization reveal novel therapeutic mechanism against stroke. *Int. J. Mol. Sci.* 18:2135. doi: 10.3390/ijms18102135
- Karch, R., Neumann, F., Neumann, M., and Schreiner, W. (1999). A three-dimensional model for arterial tree representation, generated by constrained constructive optimization. *Comput. Biol. Med.* 29, 19–38. doi: 10.1016/S0010-4825(98)00045-6
- Klyachko, V. A., and Stevens, C. F. (2003). Connectivity optimization and the positioning of cortical areas. *Proc. Natl. Acad. Sci. U.S.A.* 100, 7937–7941. doi: 10.1073/pnas.0932745100
- Kohonen, T. (1990). The self-organizing map. *Proc. IEEE* 78, 1464–1480. doi: 10.1109/5.58325
- Kremer, Y., Léger, J. F., Goodman, D., Brette, R., and Bourdieu, L. (2011). Late emergence of the vibrissa direction selectivity map in the rat barrel cortex. *J. Neurosci.* 31, 10689–10700. doi: 10.1523/JNEUROSCI.6541-10.2011
- Kumar, B. S., Khot, A., Chakravarthy, V. S., and Pushpavanam, S. (2021a). A network architecture for bidirectional neurovascular coupling in rat whisker barrel cortex. *Front. Comput. Neurosci.* 15:51. doi: 10.3389/fncom.2021.638700
- Kumar, B. S., Mayakkannan, N., Manojna, N. S., and Chakravarthy, V. S. (2021b). Artificial neurovascular network (ANVN) to study the accuracy vs. efficiency trade-off in an energy dependent neural network. *Sci. Rep.* 11:13808. doi: 10.1038/s41598-021-92661-7
- Kumar, B. S., Menon, S. C., Sriyaand, R. G., and Chakravarthy, V. S. (2022). The influence of neural activity and neural cytoarchitecture on cerebrovascular arborization: a computational model. *bioRxiv* [Preprint]. doi: 10.1101/2022.03.14.484189
- Kwon, S. E., Tsytsarev, V., Erzurumlu, R. S., and O'Connor, D. H. (2018). Organization of orientation-specific whisker deflection responses in layer 2/3 of mouse somatosensory cortex. *Neuroscience* 368, 46–56. doi: 10.1016/j.neuroscience.2017.07.067
- Lacoste, B., Comin, C. H., Ben-Zvi, A., Kaeser, P. S., Xu, X., Costa, L. F., et al. (2014). Sensory-related neural activity regulates the structure of vascular networks in the cerebral cortex. *Neuron* 83, 1117–1130. doi: 10.1016/j.neuron.2014.07.034
- Lacoste, B., and Gu, C. (2015). Control of cerebrovascular patterning by neural activity during postnatal development. *Mech. Dev.* 138, 43–49. doi: 10.1016/j.mod.2015.06.003
- Lattera, J., and Goldstein, G. W. (1991). Astroglial-induced *in vitro* angiogenesis: requirements for RNA and protein synthesis. *J. Neurochem.* 57, 1231–1239. doi: 10.1111/j.1471-4159.1991.tb08284.x
- Lattera, J., Guerin, C., and Goldstein, G. W. (1990). Astrocytes induce neural microvascular endothelial cells to form capillary-like structures *in vitro*. *J. Cell. Physiol.* 144, 204–215. doi: 10.1002/jcp.1041440205
- Lee, L. J., Iwasato, T., Itoharu, S., and Erzurumlu, R. S. (2005). Exuberant thalamocortical axon arborization in cortex-specific NMDAR1 knockout mice. *J. Comp. Neurol.* 485, 280–292. doi: 10.1002/cne.20481
- Lugo-Hernandez, E., Squire, A., Hagemann, N., Brenzel, A., Sardari, M., Schlechter, J., et al. (2017). 3D visualization and quantification of microvessels in the whole ischemic mouse brain using solvent-based clearing and light sheet microscopy. *J. Cereb. Blood Flow Metab.* 37, 3355–3367. doi: 10.1177/0271678X17698970
- Moore, C. I., and Cao, R. (2008). The hemo-neural hypothesis: on the role of blood flow in information processing. *J. Neurophysiol.* 99, 2035–2047. doi: 10.1152/jn.01366.2006
- Muddapu, V. R., Dharshini, S. A. P., Chakravarthy, V. S., and Gromiha, M. M. (2020). Neurodegenerative diseases – Is metabolic deficiency the root cause? *Front. Neurosci.* 14:213. doi: 10.3389/fnins.2020.00213
- Ogunshola, O. O., Stewart, W. B., Mihalcik, V., Solli, T., Madri, J. A., and Ment, L. R. (2000). Neuronal VEGF expression correlates with angiogenesis in postnatal developing rat brain. *Dev. Brain Res.* 119, 139–153. doi: 10.1016/S0165-3806(99)00125-X
- Paredes, I., Himmels, P., and Ruiz de Almodóvar, C. (2018). Neurovascular communication during CNS development. *Dev. Cell* 45, 10–32. doi: 10.1016/j.devcel.2018.01.023
- Peguera, B., Segarra, M., and Acker-Palmer, A. (2021). Neurovascular crosstalk coordinates the central nervous system development. *Curr. Opin. Neurobiol.* 69, 202–213. doi: 10.1016/j.conb.2021.04.005
- Peyrounette, M., Davit, Y., Quintard, M., and Lorthois, S. (2018). Multiscale modelling of blood flow in cerebral microcirculation: details at capillary scale control accuracy at the level of the cortex. *PLoS One* 13:e0189474. doi: 10.1371/journal.pone.0189474
- Plate, K. H., Breier, G., Weich, H. A., Mennel, H. D., and Risau, W. (1994). Vascular endothelial growth factor and glioma angiogenesis: coordinate induction of VEGF receptors, distribution of VEGF protein and possible *in vivo* regulatory mechanisms. *Int. J. Cancer* 59, 520–529. doi: 10.1002/ijc.2910590415
- Pradhan, R. K., and Chakravarthy, V. S. (2011). Informational dynamics of vasomotion in microvascular networks: a review. *Acta Physiol.* 201, 193–218. doi: 10.1111/j.1748-1716.2010.02198.x
- Ramoin y Cajal, S. (1995). *Histology of the Nervous System of Man and Vertebrates*. Available online at: <https://global.oup.com/academic/product/histology-of-the-nervous-system-of-man-and-vertebrates-9780195074017> (accessed November 23, 2021).
- Shabir, O., Berwick, J., and Francis, S. E. (2018). Neurovascular dysfunction in vascular dementia, Alzheimer's and atherosclerosis. *BMC Neurosci.* 19:62. doi: 10.1186/s12868-018-0465-5
- Shabudin, A., Mokhtarudin, M. J. M., El-Bouri, W. K., Payne, S. J., Naim, W. N. W. A., and Mohamed, N. A. N. (2021). “Multiscale modelling of 3-dimensional brain tissue with capillary distribution,” in *Proceedings of the 2020 IEEE-EMBS Conference on Biomedical Engineering and Sciences (IECBES)*, Langkawi Island, 315–318. doi: 10.1109/IECBES48179.2021.9398791

- Shiple, R. J., Smith, A. F., Sweeney, P. W., Pries, A. R., and Secomb, T. W. (2020). A hybrid discrete-continuum approach for modelling microcirculatory blood flow. *Math. Med. Biol. J. IMA* 37, 40–57. doi: 10.1093/IMAMMB/DQZ006
- Shweiki, D., Itin, A., Soffer, D., and Keshet, E. (1992). Vascular endothelial growth factor induced by hypoxia may mediate hypoxia-initiated angiogenesis. *Nature* 359, 843–845. doi: 10.1038/359843a0
- Tourigny, D. S., Karim, M. K. A., Echeveste, R., Kotter, M. R. N., and O'Neill, J. S. (2019). Energetic substrate availability regulates synchronous activity in an excitatory neural network. *PLoS One* 14:e0220937. doi: 10.1371/journal.pone.0220937
- Tsai, P. S., Kaufhold, J. P., Blinder, P., Friedman, B., Drew, P. J., Karten, H. J., et al. (2009). Correlations of neuronal and microvascular densities in murine cortex revealed by direct counting and colocalization of nuclei and vessels. *J. Neurosci.* 29, 14553–14570. doi: 10.1523/JNEUROSCI.3287-09.2009
- Vanzetta, I., Slovín, H., Omer, D. B., and Grinvald, A. (2004). Columnar resolution of blood volume and oximetry functional maps in the behaving monkey: implications for fMRI. *Neuron* 42, 843–854. doi: 10.1016/j.neuron.2004.04.004
- Verisokin, A. Y., Vervevko, D. V., Postnov, D. E., and Brazhe, A. R. (2021). Modeling of astrocyte networks: toward realistic topology and dynamics. *Front. Cell. Neurosci.* 15:645068. doi: 10.3389/fncel.2021.645068
- Wen, Q., and Chklovskii, D. B. (2008). A cost-benefit analysis of neuronal morphology. *J. Neurophysiol.* 99, 2320–2328. doi: 10.1152/jn.00280.2007
- Wen, Q., Stepanyants, A., Elston, G. N., Grosberg, A. Y., and Chklovskii, D. B. (2009). Maximization of the connectivity repertoire as a statistical principle governing the shapes of dendritic arbors. *Proc. Natl. Acad. Sci. U.S.A.* 106, 12536–12541. doi: 10.1073/pnas.0901530106
- Whiteus, C., Freitas, C., and Grutzendler, J. (2014). Perturbed neural activity disrupts cerebral angiogenesis during a postnatal critical period. *Nature* 505, 407–411. doi: 10.1038/nature12821
- Wizigmann-Voos, S., Plate, K. H., Breier, G., and Risau, W. (1995). Up-regulation of vascular endothelial growth factor and its receptors in von Hippel-Lindau disease-associated and sporadic Hemangioblastomas. *Cancer Res.* 55, 1358–1364.
- Woolsey, T. A., Rovainen, C. M., Cox, S. B., Henegar, M. H., Liang, G. E., Liu, D., et al. (1996). Neuronal units linked to microvascular modules in cerebral cortex: response elements for imaging the brain. *Cereb. Cortex* 6, 647–660. doi: 10.1093/cercor/6.5.647
- Wu, J., Guo, C., Chen, S., Jiang, T., He, Y., Ding, W., et al. (2016). Direct 3D analyses reveal barrel-specific vascular distribution and cross-barrel branching in the mouse barrel cortex. *Cereb. Cortex* 26, 23–31. doi: 10.1093/cercor/bh u166
- Zhang, M. Q., Sun, D. N., Xie, Y. Y., Peng, G. Y., Xia, J., Long, H. Y., et al. (2014). Three-dimensional visualization of rat brain microvasculature following permanent focal ischaemia by synchrotron radiation. *Br. J. Radiol.* 87:20130670. doi: 10.1259/bjr.20130670

Conflict of Interest: The authors declare that the research was conducted in the absence of any commercial or financial relationships that could be construed as a potential conflict of interest.

Publisher's Note: All claims expressed in this article are solely those of the authors and do not necessarily represent those of their affiliated organizations, or those of the publisher, the editors and the reviewers. Any product that may be evaluated in this article, or claim that may be made by its manufacturer, is not guaranteed or endorsed by the publisher.

Copyright © 2022 Kumar, Menon, Gayathri and Chakravarthy. This is an open-access article distributed under the terms of the Creative Commons Attribution License (CC BY). The use, distribution or reproduction in other forums is permitted, provided the original author(s) and the copyright owner(s) are credited and that the original publication in this journal is cited, in accordance with accepted academic practice. No use, distribution or reproduction is permitted which does not comply with these terms.